A SUBOPTIMAL CONTROL STRATEGY FOR A SLIDER CRANK WAVE ENERGY CONVERTER POWER TAKE-OFF SYSTEM

A thesis presented to the faculty of the Graduate School of
Western Carolina University in partial fulfillment of the
requirements for the degree of Master of Science in Technology.

By

Yuanrui Sang

Director: Dr. H. Bora Karayaka
Assistant Professor
Department of Engineering and Technology

Committee Members:
Dr. Yanjun Yan, Department of Engineering and Technology
Dr. James Z. Zhang, Kettering University

March 2015

To my families, for their endless support.

ACKNOWLEDGEMENTS

First and foremost, I would like to thank my advisor, Dr. Hayrettin Bora Karayaka, whose guidance and support have made all this work possible. I'm really grateful that he introduced ocean wave energy extraction to me, and gave me this valuable opportunity to work on this fantastic topic. It has been a rewarding experience to work with Dr. Karayaka both technically and non-technically. His passion for research has always been an inspiration and encouragement for me. He is always willing to help, and I benefited a lot from our discussions. I also took his power system analysis and power electronics courses, in which I learned a lot.

I would also like to thank my committee member, Dr. Yanjun Yan, for her help with my research. She was always there when I needed to discuss a problem with me; she also gave me some suggestions on how to organize Matlab codes and make them ran more efficiently. She also taught two graduate courses that I took and I benefited a lot from her teaching.

My thanks also goes to the other committee member of mine, Dr. James Z. Zhang, former dean of Kimmel School. Busy as he was, he never rejected me whenever I needed to talk to him about my research. He was also one of the professors who helped me set the direction of my research, and mentioned some methods to handle irregular wave energy extraction. I also benefited from the Random Variables and Stochastic Processes course he taught, and from his inspiring personal character.

I would like to extend my thanks to all the other professors who taught and helped me during my graduate years, Dr. Cory Howk, Dr. Paul Yanik, Dr. Robert Adams, Dr. Weiguo (Bill) Yang and Dr. Martin Tanaka. I benefited a lot from their classes and enjoyed their different ways of teaching. I would also like to thank Dr. Peter Tay, who provided me with instructions on formatting the thesis in Latex. I would also like to thank all my classmates in the Master of Science in Technology program, including those who graduated one year

before me and those who will graduate one year after me, for the beneficial discussions we had together.

At last, I would like to thank my families for their endless support.

TABLE OF CONTENTS

LIST OF TABLES

LIST OF FIGURES

ABSTRACT

A SUBOPTIMAL CONTROL STRATEGY FOR A SLIDER CRANK WAVE ENERGY CONVERTER POWER TAKE-OFF SYSTEM

Yuanrui Sang, M.S.T.

Western Carolina University (March 2015)

Director: Dr. H. Bora Karayaka

Ocean wave energy extraction is one of the emerging fields in renewable energy research. With high availability, high power density, high efficiency and low cost, a good prospect can be foreseen for its industrial application. Among all Wave Energy Converters (WEC), the Slider-Crank WEC stands out with its suitability for large scale WEC deployments ($> 10kW$). However, the nonlinearity of Slider-Crank system causes difficulty in controlling and maximizing energy extraction. This research develops a novel control algorithm for the generator in order to reach resonance with wave excitation force; the research is carried out under regular and irregular wave conditions, respectively. Simulation results validate that a suboptimal energy extraction can be achieved.

CHAPTER 1: INTRODUCTION

Ocean wave energy extraction is one of the emerging fields in renewable energy research. According to National Oceanic and Atmospheric Administration (NOAA), 71% of the Earths surface is covered with water [1]. Vast oceans and seas create a network of bodies of water that encompasses the globe; winds whipping across the surface of the ocean generate large open ocean waves that propagate throughout this vast network of water. These waves can travel miles with minimal energy loss in the open seas, and energy inside the waves can be captured to generate massive amount of electrical power. It's estimated that if 0.2% of ocean's energy can be extracted, it would be able to produce enough power for the whole world. Ocean wave energy features not only high availability, but also high power density, typically $30kW/m$, and good forecastability, which is 10 hours or more. Compared with wind and solar energy, ocean wave energy also has a higher conversion efficiency [2]. In addition to the advantages mentioned above, it also causes low impact to the environment, which makes it an attractive field for renewable energy research. However, at present, ocean wave energy is the most expensive type of water power because of a lack of available models of wave energy converters (WECs) [3].

Currently, there are a number of methods for converting ocean wave energy into electrical power. The methods or devices, if categorized based on the underlying basic concepts that define the systems operation, can be classified as Oscillating Water Columns, Overtopping Devices, and Oscillating Bodies, which include Heaving Devices, Pitching Devices and Surging Devices [4,5]. The first category, Oscillating Water Columns, refers to partially submerged structures open to the seabed below the water line. The linear up and down motion generated on the sea surface alternately pressurize and depressurize the air inside the structure, generating a reciprocating flow through a turbine installed beneath the roof of the device. Overtopping Devices collect water from incident waves in an elevated reservoir, and the water collected is then fed through the turbine back to the ocean with the effect of

gravity. Oscillating body uses an arrangement of physical structures to move with the waves, and the kinetic energy is converted into electrical energy with direct or indirect techniques. In this category, Heaving Devices, floating or submerged, provide a heave motion that is converted by mechanical and/or hydraulic systems into linear or rotational motion, more commonly linear, for driving electric generators. Pitching Devices consist of a number of floating bodies hinged together across their beams. Relative motion between the interconnected bodies pumps high pressure oil through hydraulic motors which drive the generators. Surging Devices employ methods that exploit the horizontal particle velocity in a wave to drive a deflector or to generate pumping effect of a flexible bag facing the wave front. Most of these devices implement a linear generator to generate electricity. Recent research and commercial applications in ocean wave energy converters can be found in references [6–16].

The slider crank Power Take-Off System (PTOS) is a type of Direct-Drive Rotational (DDR) PTOS. As shown in Figure 1.1 [17] , the ocean waves exerts an excitation force on the buoy, and the up and down movement of the buoy is converted into rotational motion through the slider-crank linkage system and a gear box so that a generator can be driven to produce electricity. It converts ocean wave energy directly to electrical power without intermediate stages involving hydraulics or pneumatics, attracting increasing attention from researchers because of its potential of high efficiency and reliability [18]. At present, most direct drive ocean wave conversion systems utilize linear generators to generate electricity. For large scale WEC deployments ($> 10kW$), a recent study [18] showed that linear generators would encounter air-gap tolerance and linear guidance challenges that would be very difficult to solve in a cost-effective way. In addition, it was found in [18] that energy capture of DDR system is higher compared with linear generator systems. As a DDR system, slider crank WEC features fixed amplitude motion, which eliminates the need for additional latching control technique to limit buoy motion under extremely high wave conditions [19]. Also, the slider crank is a proven mechanical linkage system with a history of more than 2,000 years [20–22], and it features simple structure and easy maintenance. This research investigates the feasibility of efficiently converting the heave motion of ocean waves into rotational motion

via a slider crank mechanism. To the best of our knowledge, no such analysis has been performed so far.

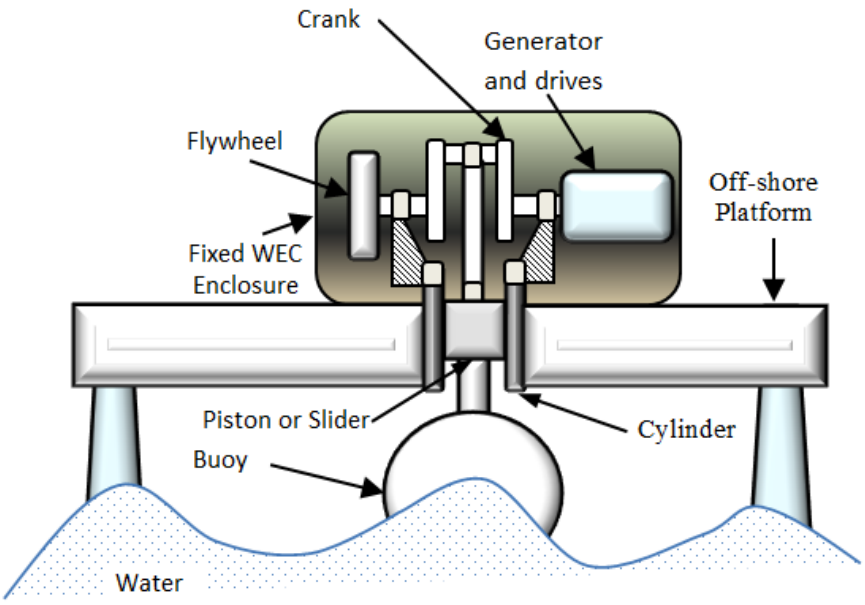

Figure 1.1: The structure of slider-crank system

This thesis proposes a nonparametric suboptimal control strategy for the slider crank WEC, which keeps the generator and the wave excitation force in resonance. The WEC and PTOS are modeled with an electrical analogue, so a mathematical model of the system can be built. Then simulations are carried out with Matlab/Simulink to validate the feasibility of the system. The research is conducted with four steps: first, the feasibility of the proposed control strategy with this system is validated under regular sinusoidal wave conditions with a DC machine in the PTOS, assuming linear PTOS interactions and utilizing frequency domain analysis; second, under regular sinusoidal wave conditions with an AC synchronous machine in the PTOS, using time-domain analysis which is suitable for nonlinear PTOS dynamics; third, under irregular wave conditions with a DC machine in the PTOS, using time-domain analysis; fourth, under irregular wave conditions with an AC synchronous machine in the PTOS, using time-domain analysis.

The rest of the thesis is organized as follows: Chapter 2 presents the models of the WEC and PTOS; chapter 3 describes the control strategy of the system; chapter 4 shows

the simulation results and analysis; chapter 5 is the conclusion and future work.

CHAPTER 2: BACKGROUND

2.1 Overall System Model

The proposed system highly resembles that of a single cylinder internal combustion engine. The basic parts of the system include a piston or slider, a connecting rod, a crank and a buoy. Aside from the buoy, these basic components are the same as those of internal combustion engines. The piston or slider is firmly affixed to a buoyant wave energy capture device which tracks the relative heave motion of ocean waves. The force that is exerted on the buoy pushes the connecting rod to turn the crank up (or down; depending on the PTOS orientation) and develops the necessary torque that drives the generator to start turning and continue the rotational motion. The physical model of the system with defining angular relationships and system variables is described in Figure 2.1 [23, 24].

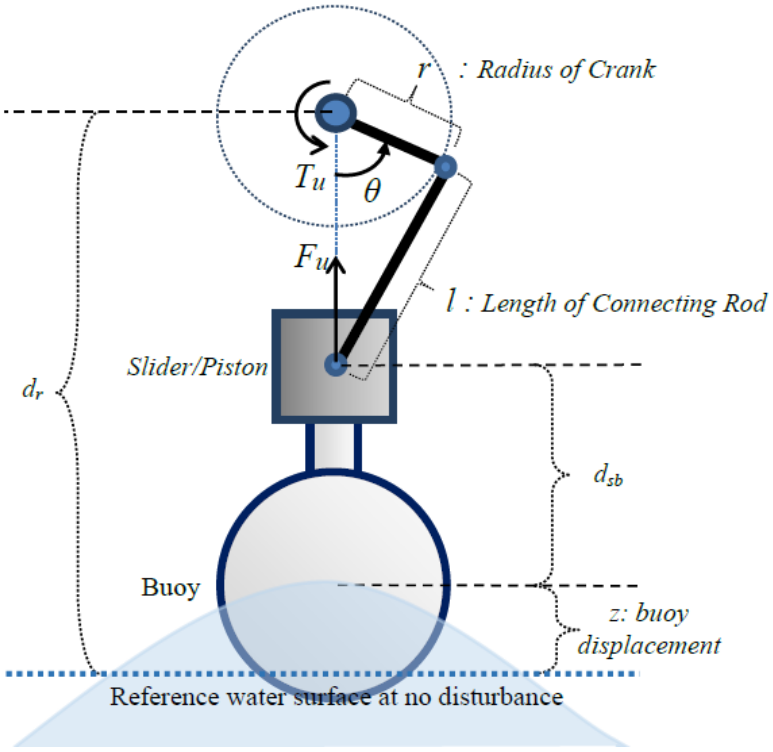

Figure 2.1: An Illustration of The Slider-Crank System

2.2 Hydrodynamics Model

In this research, a popular semi-submerged spherical buoy was selected for analysis. System operation under both regular wave conditions and irregular wave conditions were investigated. Two types of models to calculate the hydrodynamic forces were adopted. The first one was a simplified version, which assumed that the PTOS force was linear. The second one adopted time-domain analysis, in order to handle nonlinearity. In this section, wave excitation force calculation under both regular wave conditions and irregular wave conditions as well as the two methods to calculate radiation force will be introduced.

2.2.1 Wave Excitation Force Calculation For Regular Waves

When a regular sinusoidal ocean wave is adopted as the excitation source, wave elevation has the following form:

$$z_w = Asin(\omega t + \phi) \tag{2.1}$$

where A is the amplitude of wave, ω is wave angular velocity and ϕ is the initial phase of the wave.

The wave excitation force for a semi-submerged sphere of radius a due to incident wave is calculated as

$$F_e = \kappa \rho g \pi a^2 z_w \tag{2.2}$$

where z_w is water surface elevation and κ is the excitation force coefficient, whose amplitude is calculated as

$$|\kappa| = \sqrt{\frac{4\epsilon_r}{3\pi ka}} \tag{2.3}$$

in which the radiation resistance coefficient $\epsilon_r(ka)$ is a function of the product of k and a and can be calculated as suggested in the literature [25, 26] and the phase angle of κ was assumed to be zero due to the small values of ka used in this study [25].

For infinite water depth, wave number k can be calculated as

$$k = \frac{\omega^2}{g} = \frac{2\pi}{\lambda} \tag{2.4}$$

where ω is wave angular velocity and λ is wave length.

2.2.2 Wave Excitation Force Calculation For Irregular Waves

An irregular wave can be composed by a number of regular sinusoidal waves with different amplitudes, angular velocities and phases. In this research, the angular velocity is chosen in the range of 0.5 to 1.4 radian/s with an interval of 0.01 radian/s, and the interval is denoted as Δf. The amplitudes of irregular waves were generated with the JONSWAP spectrum which can be expressed as [27, 28]

$$S(f) = \frac{\alpha_j g^2}{(2\pi)^4} f^{-5} exp\Big[-\frac{5}{4}\Big(\frac{f_p}{f}\Big)^4\Big]\gamma^{\Gamma} \tag{2.5}$$

where α_j is a nondimensional variable that is a function of the wind speed and fetch length, f_p is the peak frequency of the irregular wave, f is the frequencies of the wave components, γ^{Γ} is the peak enhancement factor. A value of 6 is used for γ in this study, and

$$\Gamma = exp\Big[-\Big(\frac{\frac{f}{f_p}-1}{\sqrt{2}\sigma}\Big)^2\Big], \quad \sigma = \begin{cases} 0.07 f \le f_p \\ 0.09 f > f_p \end{cases} \tag{2.6}$$

$$\alpha_j = \frac{H_{m0}^2}{16\int_0 S^*(f)df} \tag{2.7}$$

In the above equation, H_{m0} is the significant wave height of the irregular wave, and

$$S^*(f) = \frac{g^2}{(2\pi)^4} f^{-5} exp\Big[-\frac{5}{4}\Big(\frac{f_p}{f}\Big)^4\Big]\gamma^{\Gamma} \tag{2.8}$$

In order to make it easier to compare energy extraction between regular sinusoidal waves and irregular waves, significant wave heights in the simulations can be chosen according to the equal energy transport theorem [29]:

$$H_{m0} = 2\sqrt{2}A \tag{2.9}$$

where A is the amplitude of the regular sinusoidal wave with equal energy.

The JONSWAP spectrum with a significant wave height of 1.4142 meters, which is equivalent to an amplitude of 0.5 meters for a regular wave, a peak period of 8 seconds and γ of 6 is shown in Figure 2.2.

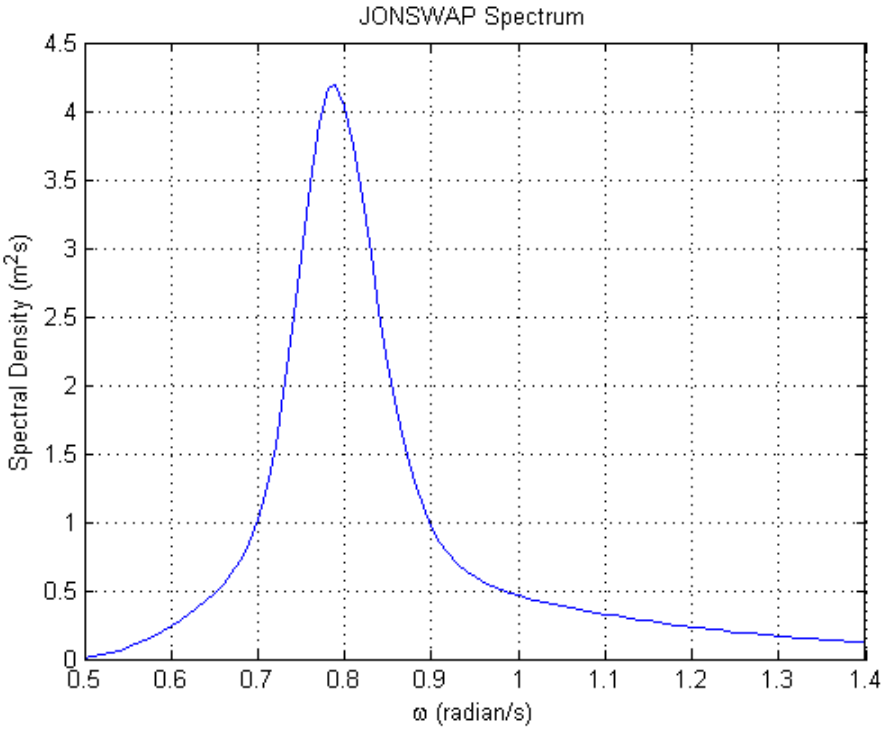

Figure 2.2: An example of the JONSWAP spectrum

The amplitude of each component of the irregular wave can thus be expressed as [30]

$$A_i = \sqrt{2S(f_i)\Delta f} \tag{2.10}$$

The phase of each component of the irregular wave is randomly generated from 0 to π, and its denoted as ϕ_i in this thesis.

Thus, the irregular wave elevation can be expressed as the summation of all the wave components

$$z_w = \sum_{i=1}^{N} A_i sin(\omega_i t + \phi_i) \tag{2.11}$$

where N is the total number of wave components.

The wave excitation force due to incident wave is calculated as

$$F_e = |\kappa|\rho g\pi a^2 z_w \angle\phi_\kappa \tag{2.12}$$

where z_w is water surface elevation and κ is the excitation force coefficient [31], whose amplitude, imaginary and real parts are calculated as

$$|\kappa| = \sqrt{\frac{4\epsilon_r}{3\pi ka}} \tag{2.13}$$

$$Im(\kappa) = \frac{2\epsilon_r ka}{3} \tag{2.14}$$

$$Re(\kappa) = \sqrt{|\kappa|^2 - [Im(\kappa)]^2} \tag{2.15}$$

where, assuming infinite water depth, wave number k can be calculated as

$$k = \frac{\omega^2}{g} = \frac{2\pi}{\lambda} \tag{2.16}$$

The phase angle of κ can be calculated as

$$\angle\phi_\kappa = tan^{-1}\left[\frac{Im(\kappa)}{Re(\kappa)}\right] \tag{2.17}$$

2.2.3 Frequency-domain System Analysis

The frequency domain analysis presented here is based on the assumption of infinite water depth [25]. With this approach, the radiation force on the buoy is proportional to buoy velocity, and the equation that describes the relationship between buoy motion and hydrodynamic forces can be expressed as

$$m\ddot{z} + R\dot{z} + S_b z = F_e - F_u \tag{2.18}$$

where z is the buoy center of gravity displacement in heave direction, m is the total mass of buoy, R is total damping, S_b is the hydrostatic stiffness, F_e is the wave excitation force, and F_u is the PTOS reactionary force.

For a semi-submerged buoy, assuming small buoy displacement in comparison to buoy radius, the buoyancy stiffness is

$$S_b = \rho g \pi a^2 \tag{2.19}$$

where g is the acceleration of gravity, ρ is the density of water, and a is the radius of buoy.

Assuming m_m is buoy mass and μ_r is the added mass coefficient, the total mass of buoy can be calculated as

$$m = m_m(1 + \mu_r(ka)) \tag{2.20}$$

where the semi-submerged buoy mass is

$$m_m = \rho \frac{2\pi}{3} a^3 \tag{2.21}$$

and the added mass coefficient $\mu_r(ka)$ is a function of the product of wave number k and buoy radius a, which can be calculated with data from references [25, 26].

The damping parameter R can be calculated as

$$R = R_v + R_f + \epsilon_r(ka)\omega m_m \tag{2.22}$$

where R_v is the linear viscous force coefficient, R_f is the friction force coefficient, and radiation resistance coefficient $\epsilon_r(ka)$ is a function of the product of k and a and will be calculated as suggested in literature [25, 26]. In this study, R_v and R_f are kept negligibly small in comparison with the radiation resistance term.

As an example, if $a = 5m$, $g = 9.81 m/s^2$, $\rho = 1020 kg/m^3$, $R_v = 10$, $R_f = 0$, $\omega = 1.0472 rad$, then $m = 4.1565 \times 10^5 kg$, $R = 9.3187 \times 10^4$, $S_b = 7.8589 \times 10^5 kg/s$.

2.2.4 Time-domain System Analysis

To deal with non-sinusoidal behavior, the Cummins equation [32] is introduced to describe the relationship between buoy motion and hydrodynamic forces and can be expressed as

$$(M + a_\infty)\ddot{z}(t) + \int_{-\infty}^{t} H_{rad}(t - \tau)\dot{z}(\tau)d\tau + S_b z(t) = F_e(t) - F_u(t) \tag{2.23}$$

where z is the buoy center of gravity displacement in heave direction, M is the physical mass of the buoy, and a_∞ is the buoy added mass at infinite wave period for semi-submerged sphere buoy, which is half of the physical mass [26]. H_{rad} is the radiation impulse response function for the buoy with a 5 meter radius, as Figure 2.3 shows. S_b is the hydrostatic stiffness and can be calculated using Equation 2.19, F_e is the wave excitation force and can be calculated using Equation 2.2, and F_u is the wave energy harvesting device reactionary force.

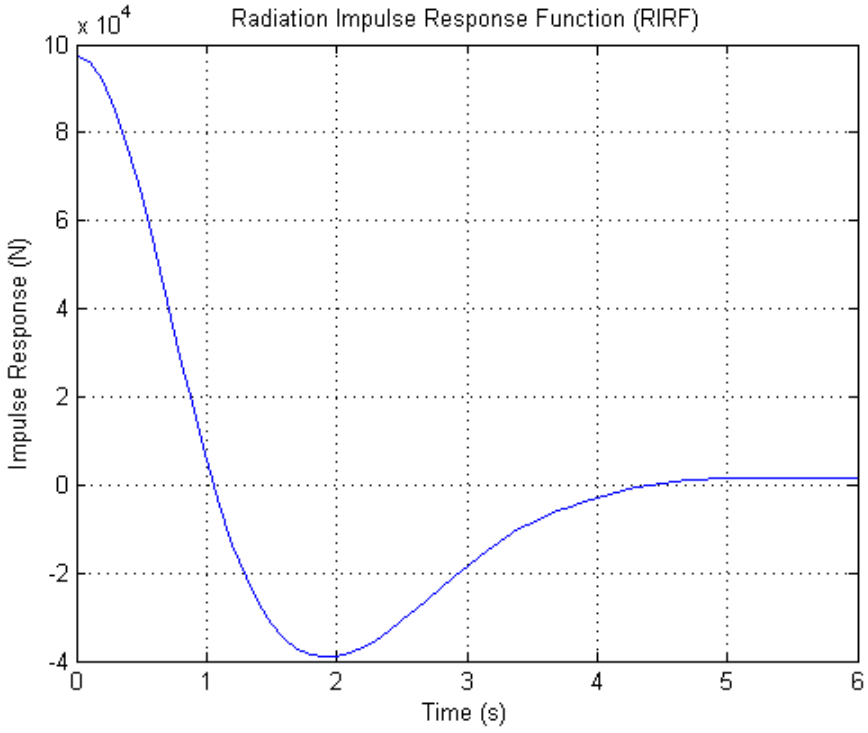

Figure 2.3: Radiation impulse response function of the buoy

The radiation force of the buoy is approximated with analytical solutions existing for the geometry [25], then a transfer function with the input of buoy velocity and the output of radiation force for a 5-meter radius semi-submerged sphere buoy is obtained through appropriate Matlab functions as follows:

$$\frac{F_{rad}}{\dot{z}} = \frac{9.7 \times 10^4 s^3 + 4.4 \times 10^5 s^2 + 7.5 \times 10^5 s - 1.6 \times 10^4}{s^4 + 4.4 s^3 + 11.2 s^2 + 12.3 s + 7.1} \tag{2.24}$$

where F_{rad} is the radiation force and $\dot{z}$ is buoy velocity. The radiation force can be mathematically expressed as

$$F_{rad} = \int_{-\infty}^{t} H_{rad}(t-\tau)\dot{z}(\tau)d\tau \tag{2.25}$$

2.3 Power Take Off System Model

In this study, two types of electric machines and relevant drive systems are adopted. One is a DC machine, because of its simplicity to model and control as well as a relatively high efficiency. The other is an AC synchronous machine, because of its efficient operational performance with DDR-WEC systems [18]; a vector controlled synchronous machine drive system in addition to a phase control algorithm is used to control the AC synchronous machine. Crankshaft torque is calculated from the hydrodynamic forces (i.e. excitation and radiation forces) and is fed into the motor drive system. Torque formulation for the slider crank mechanism involves two components [24]:

1. Drive torque:

$$T_d = F_u \cdot k(\theta, l, r) \tag{2.26}$$

2. Vibration torque:

$$T_i = (m_{cr} + m_p) \cdot [cos\theta + \lambda \cdot cos(2)] \cdot r \cdot \omega^2 \cdot k(\theta, l, r) \tag{2.27}$$

where:

$$k(\theta, l, r) = r \cdot sin\theta \cdot [1 + \lambda \cdot cos\theta/(1 - (\lambda \cdot sin\theta)^2)^{1/2}] \tag{2.28}$$

and the ratio of the crank to connecting rod length is

$$\lambda = r/l \tag{2.29}$$

The total torque function acting on the crankshaft is calculated as:

$$T_u = T_d + T_i \tag{2.30}$$

where T_u is the torque produced at the crankshaft, r is the length of the crank, l is the length of the connecting rod, F_u is the total forces acting on the slider, θ is the rotational crank angle, and mp and mcr are the mass of the piston (or slider) and connecting rod, respectively.

The generator shaft angle is obtained and fed into the hydrodynamic component (buoy), and buoy displacement is calculated by Equation 2.31 [33]. Buoy displacement is obtained from the geometric relationship between buoy displacement and the motion of the slider crank:

$$z = d_r - d_{sb} - rcos\theta - \sqrt{l^2 - (rsin\theta)^2} \tag{2.31}$$

A number of parameters of the WEC are shown in Figure 2.1, such as d_r, d_{sb}, and r.

A concern with the PTOS is the significant difference between the rated speed of the generator and the wave frequency. The frequency of real ocean waves usually lies between 1/6 Hz and 1/10 Hz, which is between 6-10 rpm if they move rotationally; whereas the speed of the generator in this study can reach up to more than 1,000 rpm. If rotating at 6-10 rpm, a commonly used rotational generator can produce very little power; thus, a gearbox is needed between the slider crank and the generator to keep the generator rotating at a speed high enough to generate electricity efficiently.

CHAPTER 3: METHODOLOGY

3.1 Equivalent Electrical Analogue of The Mechanical System

Assuming deep water and small wave amplitude, linear potential-flow theory can be applied to describe the relationship between the excitation force, hydrodynamic force and PTO force [25]. Based on this assumption, for the convenience of analysis, an electric analogue for a wave energy conversion system can be introduced to model this system, as shown in Figure 3.1 [34], and Table 3.1 [34] displays the correspondence between mechanical and electrical quantities of this system [29,34]. In this system, the hydrodynamic impedence, Z_h, is determined by the parameters of the buoy; maximum power transfer can be achieved by matching the PTO impedence, Z_u with Z_h. In [34], two control strategies are introduced. The first one is called passive loading control; Z_u only includes a resistive component in this case, and the value of Z_u equals the absolute value of Z_h. The second one is complex conjugate control, and Z_u can include both a resistive component and a reactive component; in this case, Z_u is equal to the conjugate of wave energy device impedance Z_h. In this thesis, a reactive but not complex conjugate control methodology is adopted; the reactive parts of the impedances cancels out, but the resistive parts are not equal.

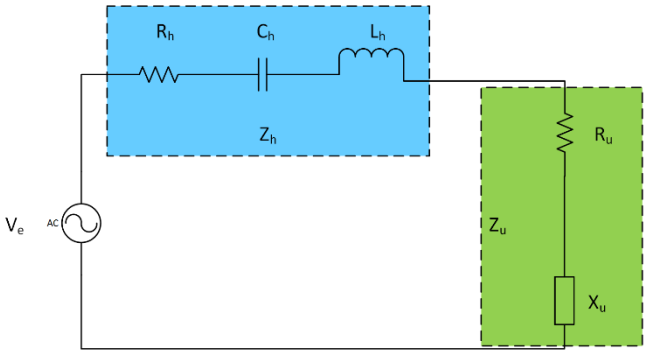

Figure 3.1: The model of the wave power conversion system

Table 3.1: The correspondence between mechanical and electrical quantities

Mechanical Domain		Electrical Domain	
Quantity	Symbol	Quantity	Symbol
Excitation force	F_e	Source voltage	V_e
Buoy velocity	$\dot{z}$	Current	i
Buoy position	z	Charge	q
WEC total mass	$M + a$ or m	Inductance	L_h
Spring Constant	S_b	Capacitance^{-1}	C_h^{-1}
Total buoy damping	R	Resistance	R_h
PTO force	F_u	Load Voltage	V_u
PTO damping	R_u	Load resistance	R_u
PTO spring constant/ PTO added mass	X_u	Load reactance	X_u

In this model, the excitation force of ocean wave, as represented by V_e, is totally uncontrollable; the spring constant, buoy damping and WEC total mass, included in Z_h, are not flexible for control either. Thus, the electric machine, which contributes to a part of the PTO impedance Z_u, is the most suitable part for control. Utilizing fast power electronics switching techniques, a control strategy can be applied to the electric machine and its characteristics can be finely tuned, thus Z_u can be adjusted. In the electric circuit analogue, with a given source voltage V_e and a constant hydrodynamic impedance Z_h, the maximum power extraction can be attained by adjusting the value of load impedance Z_u to match with Z_h. On this basis, an economically feasible method to maximize energy conversion efficiency can be established.

3.2 Operational Principles of the Slider Crank WEC

According to the electrical analogue introduced in the previous section, PTO force can be calculated as following:

$$F_u = F_e - F_h \tag{3.1}$$

in which F_h is the whole part on the left side of the Equation 2.18 or 2.23 depending on the method of hydrodynamics analysis.

A torque is developed on the crankshaft because of PTO force, thus the electric machine is driven. The speed of the electric machine can be easily measured, and converted to the speed of the slider crank:

$$\omega_{sc}(t) = \frac{\omega_m(t)}{g_r} \tag{3.2}$$

where ω_{sc} is the slider crank speed, ω_m is the motor speed and g_r is gear ratio. All the speeds are in radian/second and are functions of time.

Then the angle of the slider crank can be calculated through integration:

$$\theta = \int_0^t \omega_{sc}(t)dt \tag{3.3}$$

With the angle of slider crank, buoy displacement z can be calculated according to Equation 2.31, and then buoy velocity, $\dot{z}$, and buoy acceleration, $\ddot{z}$, can be obtained by doing 1st and 2nd order derivatives of z. With Equation 2.18 or 2.23, F_h can be calculated accordingly. Then F_u can be calculated with Equation 3.1.

A system block diagram is provided in Figure 3.2, where P_e is the electrical power output.

3.3 Control Mechanism of The Slider Crank WEC

The essence of the control strategy is to keep the generator rotate in resonance with wave excitation force. The control schematics of the Slider-Crank PTO system is shown in Figure 3.3. An angle prediction algorithm is applied on the wave excitation force, and a reference angle is produced accordingly. For regular waves, the angle prediction algorithm detects the half period and zero-crossings of wave excitation force and records the real time, then an angle reference is generated through linear extrapolation using the previous half period. For irregular waves, a half period ahead of time for the wave excitation force is assumed to be

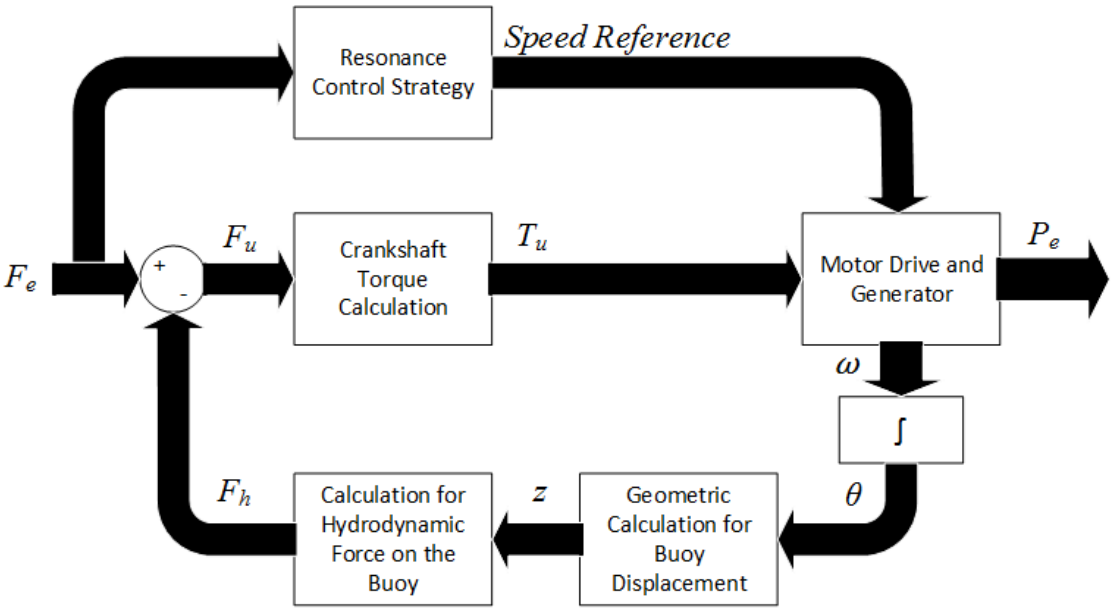

Figure 3.2: Block diagram of the system

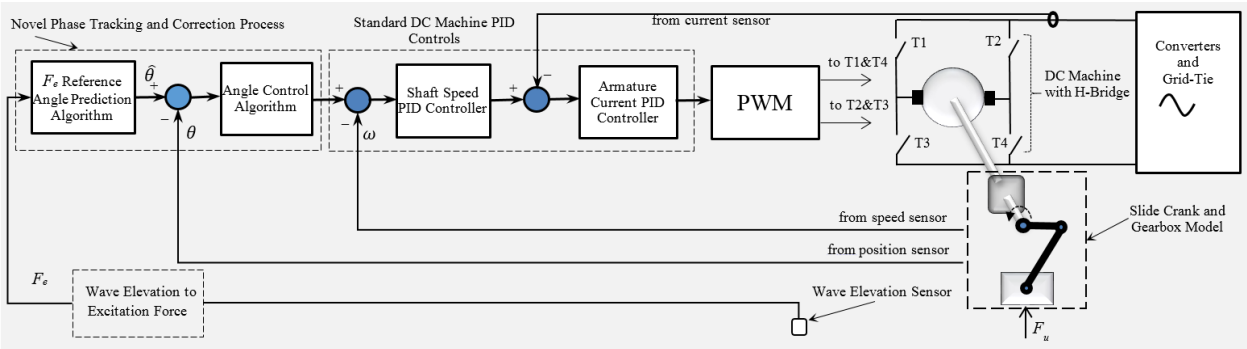

Figure 3.3: The control schematics of the Slider-Crank Wave Energy Converter

already known and selected from the off-line calculated wave excitation force, then an angle reference is generated through linear extrapolation using the future half period. For a real time control application, a prediction algorithm for the future half period of the wave excitation force would be necessary. The angle control algorithm, which is a simplified version of a PID controller, calculates a speed reference for the machine drive system based on the difference between the shaft angle and the angle reference. In this manner, continuous rotation of the generator at relatively high efficiency can be achieved. The control algorithm for regular waves is illustrated in Figure 3.4 and for irregular waves in Figure 3.5.

3.4 Discussion of Control Algorithms

Reference [29] mentioned two impedance-matching control strategies: passive loading and complex conjugate control, respectively. In these strategies, Z_h is assumed to be constant, and Z_u is controlled to optimize energy extraction. When Z_u is resistive and has the same impedance value, the energy is maximized in a passive control sense; when Z_u has a reactive component and is the complex conjugate of Z_h, energy extraction is maximized in a complex conjugate control sense. When passive control is applied, buoy velocity, $\dot{z}$, and PTOS force, F_u, are in phase; when complex conjugate control is applied, PTOS force is out of phase with buoy velocity, but the excitation force is in phase with buoy velocity.

In this study, buoy velocity is kept in phase with the excitation force; thus, the control algorithm can be considered a reactive control strategy. By keeping the excitation force and buoy velocity in phase, the algorithm ensures that the reactive part of the PTOS impedance cancels the reactive part of the characteristic impedance Z_h. Control of the resistive part of the PTOS impedance is also necessary for full complex conjugate control; however, it requires amplitude modulation of buoy motion, which cannot be achieved with a fixed radius slider crank.

An advantage of this control algorithm is that it is adaptive, which detects changes in wave excitation force periods and updates generator speed accordingly. Another advantage of this control algorithm is that it is nonparametric, and no mechanical parameter needs to be adaptively changed during the control process.

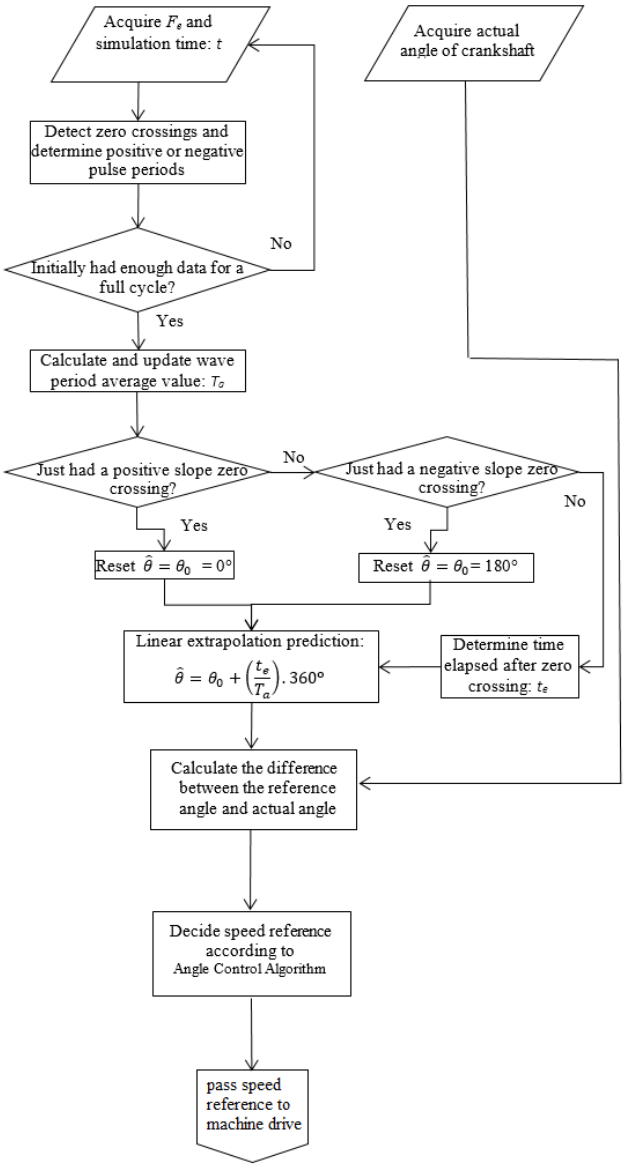

Figure 3.4: Flowchart of the control algorithm for regular waves

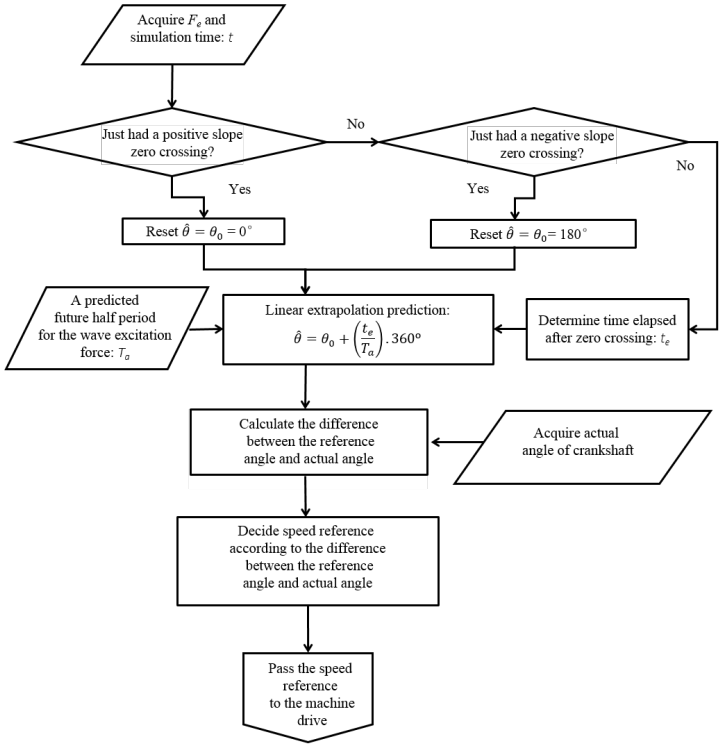

Figure 3.5: Flowchart of the control algorithm for irregular waves

CHAPTER 4: RESULTS AND DISCUSSION

4.1 Theoretical Maximum Energy Extraction

When passive loading control is applied, optimum Z_u is a purely resistive component, and its value is given by

$$R_u = \sqrt{R^2 + \left(\omega m - \frac{S_b}{\omega}\right)^2} \tag{4.1}$$

$$X_u = 0 \tag{4.2}$$

Optimal power transferred is expressed as

$$P_{passive} = \frac{F_e^2 R_u}{(R + R_u)^2 + \left(\omega m - \frac{S_b}{\omega}\right)^2} \tag{4.3}$$

When complex conjugate control is applied, the resistive and reactive components of optimum Z_u are

$$R_u = R \tag{4.4}$$

$$X_u = -\left(\omega m - \frac{S_b}{\omega}\right) \tag{4.5}$$

Optimal power transferred is given by

$$P_{optimum} = \frac{F_e^2}{4R} \tag{4.6}$$

With Equations 4.3 and 4.6, we can calculate instantaneous optimal mechanical power transfer with either passive loading or complex conjugate control strategy.

In order to compare with simulation results, in this study, rms values of optimal power transfer passive and complex conjugate control strategies were calculated for buoy radii from 1 meter to 5 meters, with generator moment of inertia of 10 $kg \cdot m^2$, under constant-frequency regular sinusoidal wave condition. The wave elevation can be expressed as

$$z_w = 0.5 sin(\frac{2\pi}{6} t) \tag{4.7}$$

which means the maximum wave elevation is 0.5 meter and wave period is 6 seconds. In rms power calculation, the rms values of F_e is used in Equations 4.3 and 4.6.

According to [35], there are two upper bounds for wave power extraction. The first one is expressed in Equation 4.8:

$$P_{upper1} = 2ak\frac{\rho}{128}\left(\frac{g}{\pi}\right)^3 T^3(2A)^2 \tag{4.8}$$

where ρ is water density, g is the gravitational acceleration, T is wave period, A is wave amplitude, k is wave number and a is buoy radius. If $T = 6s$ and $A = 0.5m$, k is calculated using Equation 2.4, and a is from 1 to 5 meters, then P_{upper1} are shown in Table 4.1.

Table 4.1: The first upper bound of power extraction for each buoy size

Buoy Radius (m)	1	2	3	4	5
$P_{upper2}(kW)$	11.72	23.43	35.15	46.87	58.59

The second upper bound is expressed in Equation 4.9:

$$P_{upper2} = \frac{2\pi\rho gAV}{4T} \tag{4.9}$$

where V is buoy volumn and it can be expressed as

$$V = \frac{4}{3}\pi a^3 \tag{4.10}$$

where a is buoy radius. If $T = 6s$ and $A = 0.5m$, and buoy radius ranges from 1 to 5 meters, the second bound for wave power extraction is shown in Table 4.2.

Table 4.2: The second upper bound of power extraction for each buoy size

Buoy Radius (m)	1	2	3	4	5
$P_{upper2}(kW)$	5.49	43.89	148.14	351.14	685.81

According to Equation 4.3 and 4.6, and applying the smaller one of the two upper bounds, theoretical values of optimum energy extraction are shown in Table 4.3.

Table 4.3: Theoretical energy extraction (rms value)

Buoy Radius (m)	1	2	3	4	5
$P_{passive}(kW)$	1.76	5.89	11.16	16.97	23.15
$P_{optimum}(kW)$	5.49	23.43	35.15	46.87	52.40

4.2 WEC Model with a DC Machine under Regular Wave Conditions

4.2.1 Simulation Setup

Simulations were carried out in Matlab/Simulink environment. Wave excitation force was calculated with Matlab and imported into the Simulink model with a *toworkspace* module, and a standard four-quadrant chopper DC drive from the *SimPowerSystems* toolbox was utilized; power produced by the generator was consumed by a braking resistor. The whole system followed the block diagram in Figure 3.2.

Under constant frequency regular wave conditions, the speed reference for the generator is constant. Thus, a steady state can be achieved when generator shaft speed reaches the reference. In steady state, the generator rotates at almost constant speed, and buoy velocity is in phase with wave excitation force. The system is able to produce power with a carefully selected PTOS gear ratio and PTOS moment of inertia. The generators moment of inertia is a constant which we cannot modify, but we can add an inertia wheel to change the inertia of the PTOS.

Simulations are implemented in the following steps. First, a simulation example with commonly used parameters is given in Section 4.2.2. Energy extraction results and system steady operation waveforms are provided, in order to verify its feasibility and suboptimal nature. Second, energy extraction from waves with different amplitudes and periods are obtained, validating that the system is suitable for waves with a wide range of amplitudes and periods. Third, the influence of PTOS gear ratio and generators moment of inertia is investigated, showing that the two parameters should be chosen according to the range of wave amplitudes and frequencies in order for the system to produce power while maintaining

system stability.

In simulations of this study, parameters in Table 4.4 and 4.5 are adopted; but wave amplitude and period, buoy size, PTOS gear ratio and PTOS moment of inertia varies in different cases of simulations, and these parameters will be specified for each case.

Table 4.4: Mechanical parameters used in simulations

Parameter	Value
r	$0.5m$
l	$1.0m$
$d_r - d_{sb}$	$1.0m$
ρ	$1020kg/m^2$
g	$9.81N/kg$
R_v	$10kg/s$
R_f	0
$m_{cr} - m_p$	$10kg$

Table 4.5: Generator parameters used in simulations

Parameter	Value
Nominal Speed	$1184rpm$
Nominal Power	$149.2kW$
Nominal Voltage	$440V$
Current Reference Limit	$1.5p.u.$
Viscous Friction Coefficient	$0.32N/(m/s)$
Armature Resistance	0.076Ω
Armature Inductance	$0.00157H$
Field Resistance	310Ω
Field Inductance	$232.25H$
Mutual Inductance	$3.320H$

4.2.2 A Simulation Example

In order to validate the feasibility of this control algorithm, a simulation example is provided as following. Given that wave amplitude is 0.5 meter, period is 6 seconds, buoy radius is 5 meters, gear ratio is 115, and generators moment of inertia is 10 $kg{\cdot}m^2$, an average mechanical

power of 38.02 kW can be transferred and an average electrical power of 32.11 kW can be produced in steady state with this resonance control strategy. The efficiency of the DC machine in this simulation case can thus be calculated as 84.47%, assuming the slider crank linkage mechanism is lossless.. The mechanical power transferred is between the maximums of passive loading and complex conjugate control strategies, thus the control strategy in this study is a suboptimal one; in the meantime, the DC machine works at an acceptable efficiency and produces a reasonable amount of electrical power.

Steady state operation of the system can be observed from Figure 4.1. From Figure 4.1(a) we can see that the fluctuation in generator shaft speed is only approximately 1 rpm. Generator shaft angle, which is in phase with wave excitation force, can be observed from Figure 4.1 (b). Figure 4.1(c) and Figure 4.1(d) shows buoy velocity and wave excitation force, respectively, and from the two plots we can see that they are in phase. There is a moderate fluctuation in the output voltage, as can be seen from Figure 4.1(f). Assuming nearly constant voltage, the output current is directly related to electrical power production, and from Figure 4.1(g) we can see that most of the time the current is positive, which means the machine generates power; but there is a small portion of time when it consumes power to satisfy reactive control methodology. The machine needs to absorb a limited amount of energy to reach steady state, as Figure 4.2 shows; in steady state, the machine produces more energy than it consumes, thus, in general, the cumulative energy produced increases as time elapses.

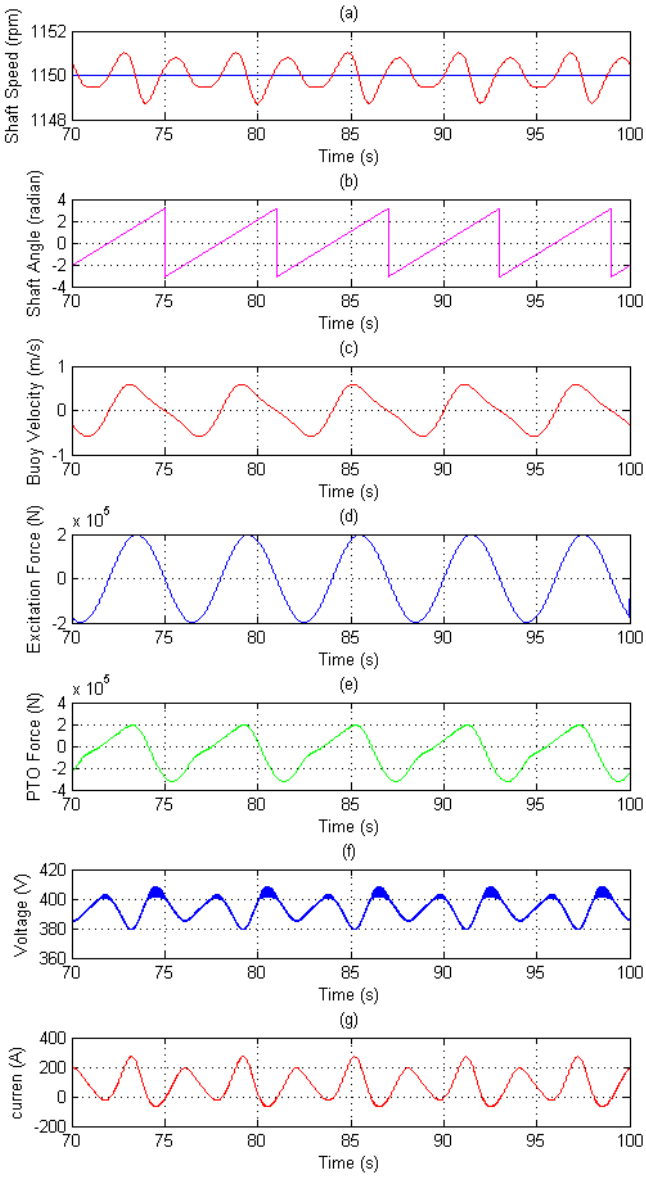

Figure 4.1: A simulation example with a DC machine and regular wave
(a) Generator shaft speed (red) and speed reference (blue).
(b) Generator shaft angle. (c) Buoy velocity.
(d) Wave excitation force. (e) PTOS force.
(f) Output voltage. (g) Output Current.
($a = 5m$, Gear ratio= 115, PTOS moment of inertia= $10kg \cdot m^2$)

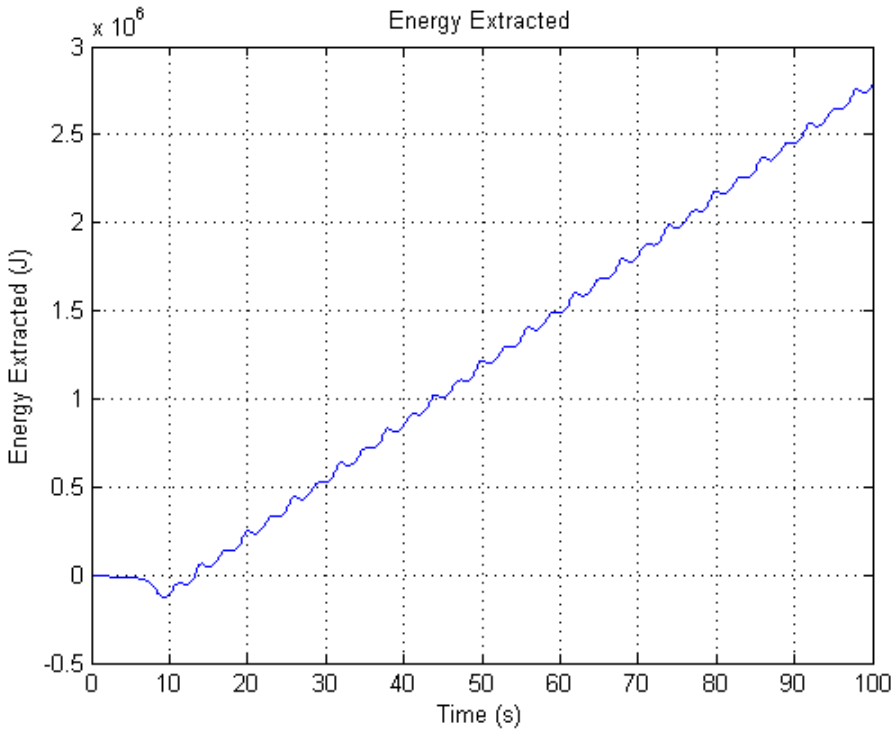

Figure 4.2: Cumulative electrical energy production with a DC machine and regular wave

4.2.3 The Influence of Wave Period and Amplitude

In this study, simulations were carried out at different wave periods and amplitudes, and Table 4.6 provides a series of average electrical power data collected at different wave periods and heights, with buoy radius of 5 meters, gear ratio of 123 and generators moment of inertia of 10 $kg \cdot m^2$. In Table 4.6, A is wave amplitude and T is wave period. The gear ratio of 123 was selected to keep system stability at a large wave period and a small PTOS moment of inertia.

Table 4.6: Average electrical power production with a DC machine at different wave periods and amplitudes of regular waves (kW) ($a = 5m$, Gear ratio= 123, PTOS moment of inertia= $10kgm^2$)

T(s) / A(m)	6	7	8	9	10
0.2	1.37	7.62	10.96	12.51	13.04
0.3	11.59	17.81	20.81	21.87	21.84
0.4	21.67	27.81	30.43	30.94	30.32
0.5	31.61	37.61	39.79	39.72	38.48

The table shows that the system can extract energy from a wide range of waves with different periods and amplitudes; suboptimal electrical power generation can be achieved even after taking generator efficiency into account. Data in the table show that energy extraction generally increases as wave amplitude and period increases; but as wave amplitude and period become too large, energy extraction does not necessarily increase as the two increase, because the current limit of the electric machine is reached and the power-producing capacity of the electric machine is saturated.

4.2.4 The influence of Gear Ratio and Inertia

From Equation 2.2, 2.3 and 2.4, it can be seen that wave excitation force is related to buoy radius, wave amplitude and wave period. Thus, if wave period, height and buoy size are kept constant, energy extracted by the WEC should also be a constant ideally. However, PTOS gear ratio imposes an influence on the amount of electricity that can be generated. Simulations are carried out at constant wave parameters, and buoy radius from 1 meter to 5 meters, at different gear ratios. The results are listed in Table 4.7.

The data in Table 4.7 show that although the average electrical power produced at different gear ratios varies, all the results are between the passive loading control maximums and the complex conjugate control maximums, which means the control strategy's suboptimal nature can be maintained for a range of gear ratios. As can be seen from Table 4.7,

each buoy size is related to a gear ratio which maximizes energy extraction.

Table 4.7: Comparison of theoretical mechanical power transfer and electrical power production in simulation ($A = 0.5m$, $T = 6s$, PTOS Inertia= $10kg \cdot m^2$)

Buoy Radius (m)	Resistive Control Power Extraction (kW)	Reactive Control Power Extraction (kW)	Gear Ratio	Electrical Power Production (kW)
1	1.76	5.49	15	2.73
			25	3.03
			50	2.56
2	5.89	23.43	40	9.94
			45	10.02
			50	10.01
3	11.16	35.15	56	18.28
			60	18.35
			100	17.08
4	16.97	46.87	84	26.28
			85	26.25
			90	26.12
5	23.15	52.40	115	32.11
			120	31.74
			155	27.08

Simulations have shown that, for a given buoy size, the system may become unstable when gear ratio is very small, and the system may consume power instead of producing it when gear ratio is very large. The effective range of gear ratios for the system, which keeps the system stable while producing power, is different for each buoy size; in general, the minimum, maximum, and optimum values of gear ratio increase as buoy size increases. Theoretical investigation into the minimum, maximum, and optimum gear ratios are beyond the scope of this study.

Furthermore, according to the simulation results, PTOS inertia also has an impact on system stability. When PTOS inertia is increased, the minimum of the effective gear ratios can be lowered. With a large-sized buoy, like one with a radius of 4 or 5 meters, the simulated system often starts oscillating before the gear ratio is lowered to one that maximizes energy extraction. If the system can be kept stable at a lower gear ratio, the optimum gear ratio can

be reached. Thus, a lowered minimum effective gear ratio helps improve energy extraction for large-sized buoys. Taking a 5-meter buoy as an example, if the excitation wave has a 0.5-meter amplitude and a 6-second period, when PTOS inertia is 10 $kg \cdot m^2$, the system is unstable when gear ratio is less than 115. However, when PTOS inertia is 25 $kg \cdot m^2$, a maximum energy extraction can be reached at a gear ratio of 80 and the system is still stable.

A similar test to the one in Section 4.2.3 is implemented with a gear ratio of 80 and PTOS moment of inertia of 25 $kg \cdot m^2$, and the results are provided in Table 4.8. From the results one can see that with an increased inertia and a lowered gear ratio, energy extraction from small-period waves is improved but is reduced from large-period ones. Thus, for real application, gear ratio should be chosen according to common periods of ocean waves, so that the system works at high efficiency for the commonly existing waves.

Table 4.8: Average electrical power production with a DC machine at different wave periods and amplitudes of regular waves (kW) ($a = 5m$, Gear ratio= 80, PTOS moment of inertia= $25kg \cdot m^2$)

T(s) / A(m)	6	7	8	9	10
0.2	3.97	9.02	11.33	12.06	11.92
0.3	13.98	18.80	20.54	20.6	19.75
0.4	23.67	28.09	29.17	28.42	27.11
0.5	33.02	36.93	37.41	36.24	34.05

4.3 WEC Model with an AC Synchronous Machine under Regular Wave Conditions

4.3.1 Simulation Setup

Wave excitation force was calculated with Matlab and imported into the Simulink model, and a standard self-controlled synchronous machine drive from the *SimPowerSystems* toolbox was utilized; power produced by the generator went back into the grid with a unity power factor. The whole system followed the block diagram shown in Figure 3.2.

In simulations of this study, parameters in Table 4.9 and 4.10 were adopted; but wave amplitude and period, buoy size and PTOS gear ratio varied in different cases of simulations and these parameters would be specified for each case.

Table 4.9: Mechanical parameters used in simulations

Parameter	Value
r	$0.5m$
l	$1.0m$
$d_r - d_{sb}$	$1.0m$
ρ	$1020kg/m^2$
g	$9.81N/kg$
R_v	$10kg/s$
R_f	0
$m_{cr} - m_p$	$10kg$
PTO Moment of Inertia	$15kg \cdot m^2$

Table 4.10: Generator parameters used in simulations

Parameter	Value
Number of Poles	6
Nominal Power	$149.2kW$
Nominal Voltage	$460V$
Viscous Friction Coefficient	$0.005N/(m/s)$
Stator Resistance	$2.01 \times 10^{-3}\Omega$
Stator Leakage Inductance	$4.289 \times 10^{-4}H$
Field Resistance	$4.083 \times 10^{-4}\Omega$
Field Leakage Inductance	$0.429 \times 10^{-3}H$
D-axis Resistance	$8.25 \times 10^{-3}\Omega$
D-axis Leakage Inductance	$0.685 \times 10^{-3}H$
Q-axis Resistance	$13.89 \times 10^{-3}\Omega$
Q-axis Leakage Inductance	$1.44 \times 10^{-3}H$
D-axis Mutual Inductance	$4.477 \times 10^{-3}H$
Q-axis Mutual Inductance	$1.354 \times 10^{-3}H$

Results from simulations are shown in the following steps. First, a simulation example with commonly used parameters is given in the next section. Energy extraction results

and system-steady operation waveforms are provided to verify its feasibility and suboptimal nature. Second, energy extraction from waves with different amplitudes and periods are obtained, validating that the system is suitable for waves with a wide range of amplitudes and periods. Third, the influence of PTOS gear ratio and the generators moment of inertia is investigated, and it is compared with previous work, the WEC system with a DC machine, showing that the two parameters have negligible influence on the vector controlled AC synchronous machine.

4.3.2 A Simulation Example

To validate the feasibility of this control algorithm, a simulation example is provided as follows. Given that wave amplitude is 0.5 meter, period is 6 seconds, buoy radius is 5 meters, gear ratio is 110, and the generators moment of inertia is 15 $kg \cdot m^2$, an average electrical power of 38.326 kW can be produced in steady state with this reactive control strategy. The electrical power produced is between the maximums of passive loading and complex conjugate control strategies and it shows that the control strategy is a suboptimal one in this case.

Steady-state operation of the system can be observed in Figure 4.3. Figure 4.3(a) shows that the fluctuation in the generator shaft speed is approximately only ± 7 rpm. Figure 4.3(b) shows crank shaft angle, which is in phase with wave excitation force. Figure 4.3(c) and Figure 4.3(d) show buoy velocity and wave excitation force, respectively; it can be seen that they are in phase as expected. There is a moderate fluctuation in the DC bus voltage, which is about ± 3 V, as shown in Figure 4.3(f). The electromagnetic torque of the generator is shown in Figure 4.3(g), and it can be seen that the torque is positive most of the time, which means the machine generates power; but there is a small portion of time when it consumes power to satisfy reactive control methodology. As Figure 4.4 shows, the machine needs to absorb a limited amount of energy to reach steady state; in steady state, the machine produces more energy than it consumes. Thus, in general, the cumulative energy produced increases as time elapses.

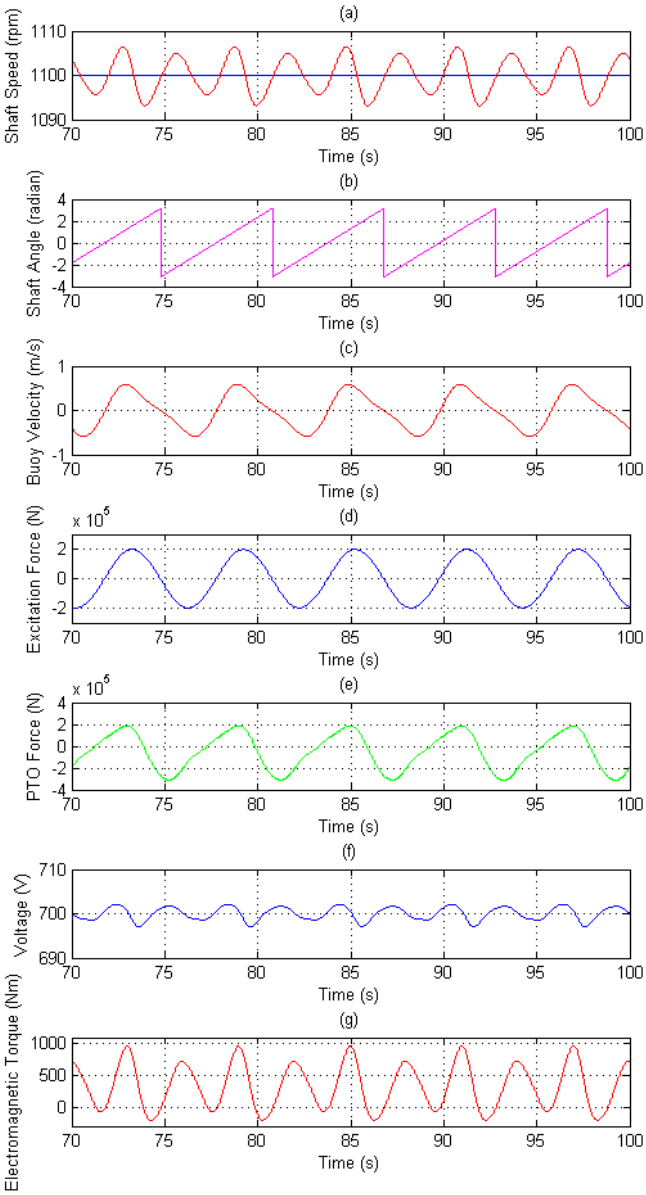

Figure 4.3: A simulation example with an AC machine and regular wave
(a) Generator shaft speed (red) and speed reference (blue).
(b) Generator shaft angle. (c) Buoy velocity.
(d) Wave excitation force. (e) PTOS force.
(f) DC bus voltage. (g) Electromagnetic torque of the generator.
($a = 5m$, Gear ratio= 110, PTOS moment of inertia= $15kg \cdot m^2$)

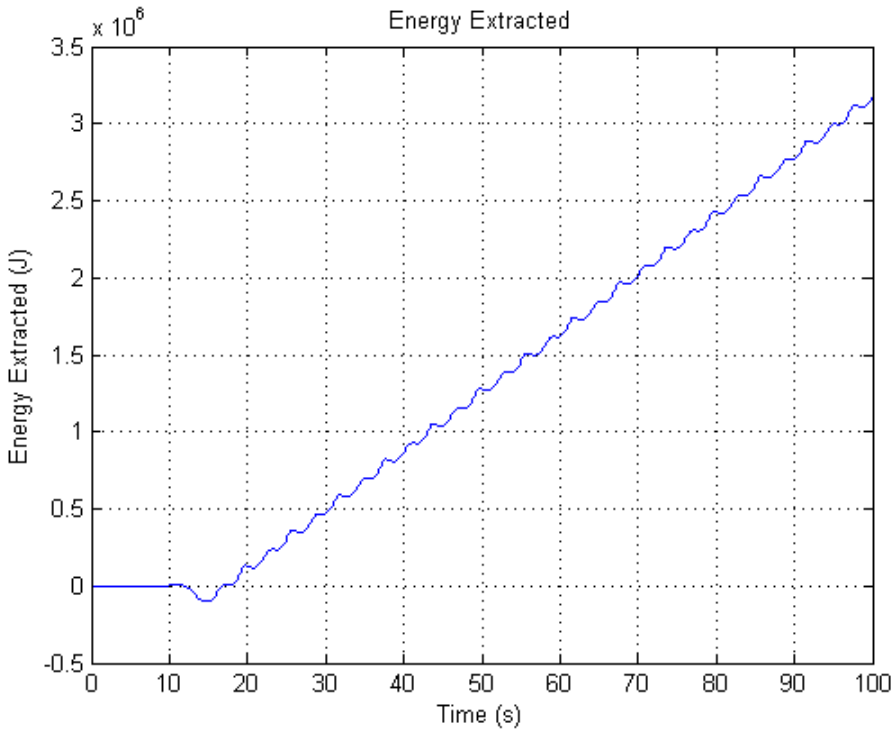

Figure 4.4: Cumulative electrical energy production with an AC machine and regular wave

4.3.3 The Influence of Wave Period and Amplitude

Observation of the simulation results shows that given the same WEC parameter, power transferred increases almost linearly as wave height increases, but does not always increase as wave period increases.

In this study, simulations are carried out at different wave periods and amplitudes, and Table 4.11 provides a series of average electrical power data collected at different wave periods and heights, with a buoy radius of 5 meters, gear ratio of 110, and the generators moment of inertia of 15 $kg{\cdot}m^2$. In Table 4.11, A is wave amplitude, and T is wave period. The wave amplitudes are kept at relatively small values because linear coefficients for excitation force and hydrostatic buoyancy force calculations can only be used when the wetted surface of the buoy is approximately constant [36].

Table 4.11: Average Electrical Power Production (kW) at Different Wave Periods and Amplitudes for AC Machine and Regular Waves ($a = 5m$, gear ratio= 110, PTOS moment of inertia= $15kgm^2$)

T(s) / A(m)	6	7	8	9	10
0.2	7.2977	12.222	14.861	16.032	16.356
0.25	12.465	17.458	20.001	20.991	21.097
0.3	17.634	22.694	25.143	25.952	25.839
0.35	22.804	27.932	30.286	30.914	30.583
0.4	27.976	33.171	35.43	35.877	35.327
0.45	33.151	38.410	40.576	40.842	40.073
0.5	38.326	43.651	45.723	45.819	44.820

The table shows that the system can extract energy from a wide range of waves with different periods and amplitudes; a suboptimal electrical power generation can be achieved. Figure 4.5 is a 3-D plot showing electrical energy production in relation to wave height and wave period according to the data in Table 4.11.

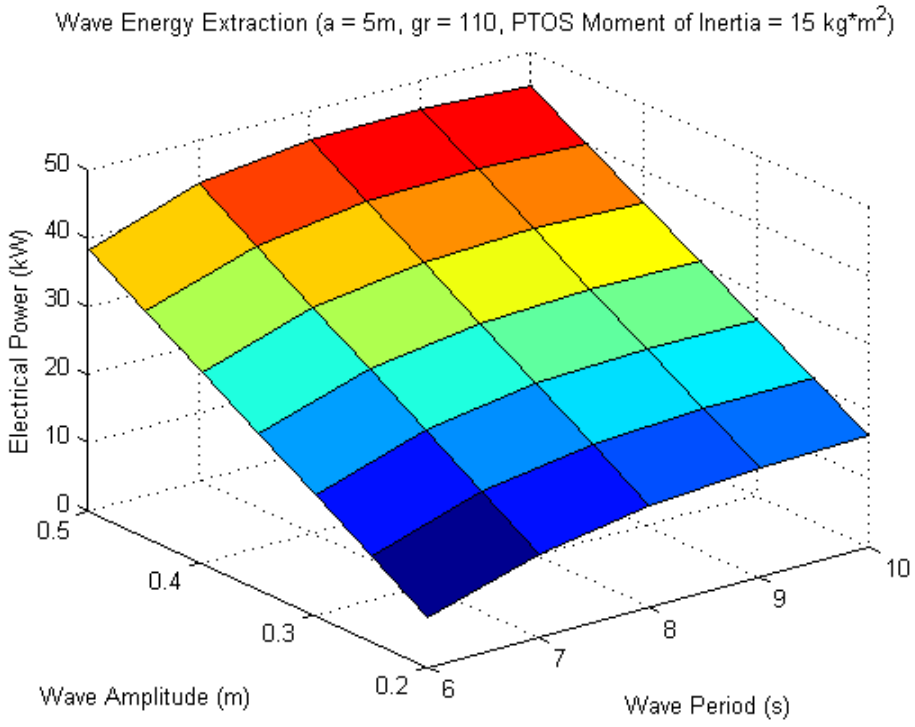

Figure 4.5: Electrical power production with an AC machine and regular waves ($a = 5m$, gear ratio= 110, PTOS moment of inertia= $15kg \cdot m^2$)

4.3.4 The influence of Gear Ratio and Inertia

As discussed in the previous section [23], for a slider crank WEC system with a DC generator, gear ratio imposes a considerable influence on the amount of energy that can be extracted, and a larger PTO moment of inertia helps increase system stability while the gear ratio is small. Thus if more energy can be extracted at a low gear ratio, an increase in PTO moment of inertia will help the system remain stable while working at such a low gear ratio. However, for the system with an AC synchronous machine, simulation data show that the influence of gear ratio on power production is minimal; also, the system can work stably at a lower gear ratio than the system with a DC generator and drive system, although it may still become unstable at very low values of gear ratio. Thus, it is unnecessary to manipulate the PTO moment of inertia to make the system work at a low gear ratio for the slider crank WEC with an AC synchronous generator and vector control drive system.

Simulations were carried out with buoy radius from 1 meter to 5 meters, each with

two different gear ratios. The results are presented in Table 4.12, and it can be seen that, for each buoy size, power production remains very close when different gear ratios are applied, and all the power production results are between the values of theoretical power production with passive loading control method and complex conjugate control method.

Table 4.12: Comparison of theoretical mechanical power transfer and electrical power production in simulation ($A = 0.5m$, $T = 6s$, PTOS Inertia= $15kg \cdot m^2$)

Buoy Radius (m)	Resistive Control Power Extraction (kW)	Reactive Control Power Extraction (kW)	Gear Ratio	Electrical Power Production (kW)
1	1.76	5.49	110	3.4179
			15	3.4879
2	5.89	23.43	110	11.425
			30	11.500
3	11.16	35.15	110	21.039
			55	21.106
4	16.97	46.87	110	30.360
			70	30.418
5	23.15	52.40	110	38.326
			90	38.362

4.4 WEC Model with a DC Machine under Irregular Wave Conditions

4.4.1 Simulation Setup

Wave excitation force array was calculated off-line according to Section 2.2.2 and imported into the Simulink model. The hydrodynamics model was also established as mentioned in Section 2.2.4. In this system, a standard four-quadrant chopper DC drive was used; power produced by the generator was consumed by a braking resistor. The nominal speed of the generator was 1184 *rpm* and the upper limit of the shaft speed of the generator was set to be 1350 *rpm* in order to protect the generator and maintain system stability. The control algorithm script was coded in Matlab and embedded into the Simulink model.

Simulation results are shown in the following steps. First, a simulation example with commonly used parameters is given in Section 4.4.2. Energy extraction results and system

operation waveforms are provided to present its feasibility. Second, system simulations are carried out with irregular waves with different significant wave heights and peak periods, validating that the system is suitable for waves with a wide range of amplitudes and periods. A discussion on the energy extraction results is provided at the end of this section.

In the simulations of this study, parameters in Table 4.4, 4.13 and 4.5 were adopted. However, the significant wave heights and peak periods associated with the irregular waves varying in different cases of simulations would be specified for each case.

Table 4.13: Additional mechanical parameters used in simulations

Parameter	Value
PTO Moment of Inertia	$10kg \cdot m^2$
PTO gear ratio	110
buoy radius (a)	5 m

4.4.2 A Simulation Example

To show the details of the system's performance, a simulation example is provided as follows. In this simulation example, the significant wave height of the irregular wave is 1.4142 meters and the peak period is 8 seconds, and the simulation is run for 500 seconds.

In order to eliminate the effects of early transients due to wave excitation force calculations, an average electrical power production is always calculated from the 100th second to the 500th second. In this case, the average electrical power production is 23.21 kW. The average mechanical power extracted by the slider crank during this period of time is 31.19 kW, thus the overall efficiency of the generator and power electronics can be calculated as 74.40%.

The wave elevation in this simulation example from the 100th second to the 500th second is shown in Figure 4.6, and the cumulative energy production during this period is shown in Figure 4.7. It can be seen that energy extraction generally increases as time elapses, although the power produced by the system can be very different at different points of time

because of the irregular wave elevations. This proves that the system produces more energy than it consumes.

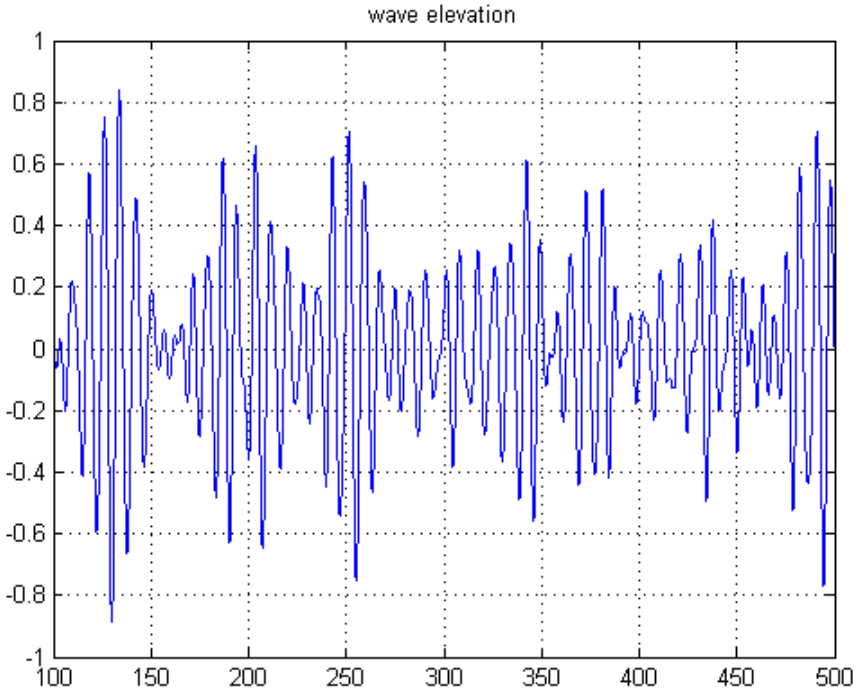

Figure 4.6: Wave elevation

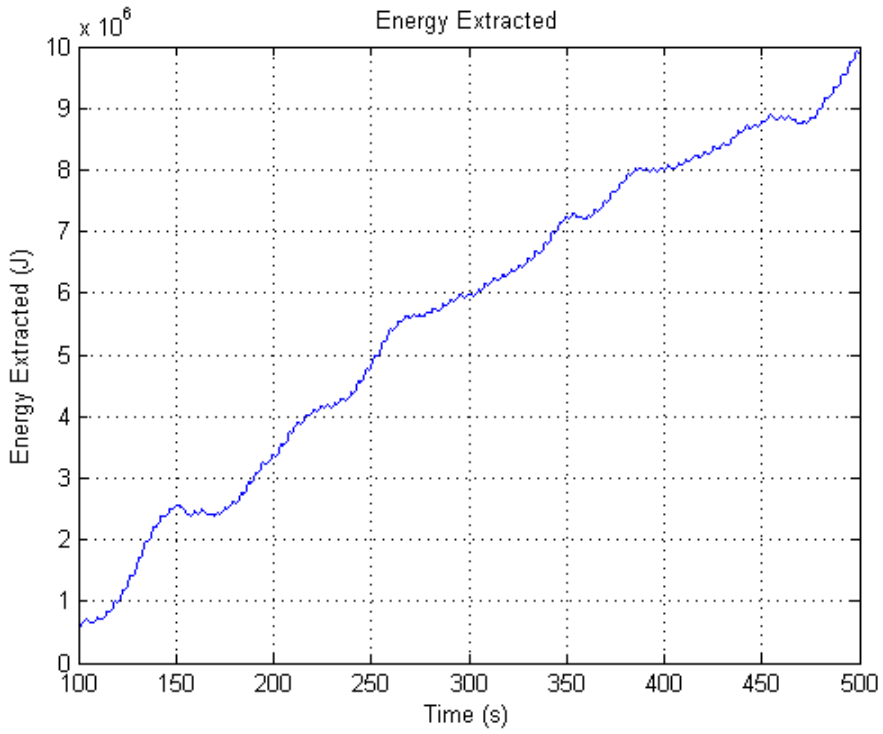

Figure 4.7: Cumulative electrical energy production with a DC machine and irregular wave

The generator shaft speed is shown in Figure 4.8. The blue curve is the shaft speed reference and the red curve is the actual generator shaft speed in the simulation. It can be seen from the figure that the control algorithm effectively maintained the generator speed consistent with its reference. Figure 4.9 shows the shaft angle of the generator, Figure 4.10 shows the buoy velocity, and Figure 4.11 shows the wave excitation force; from the three plots, it can be observed that shaft angle of the generator and buoy velocity are kept in resonance with the excitation force. The output current of the generator is shown in Figure 4.12. Because output voltage is always positive, a positive current in the plot means that the generator is producing power and a negative current means that it is consuming power to maintain its resonance with the excitation force. From the plot, one can see that while producing power, the generator needs to consume a small amount of power to keep resonance. The simulation was run for 500 seconds, but in order to show more details, simulation results from the 300th second to the 400th second are shown in this plot.

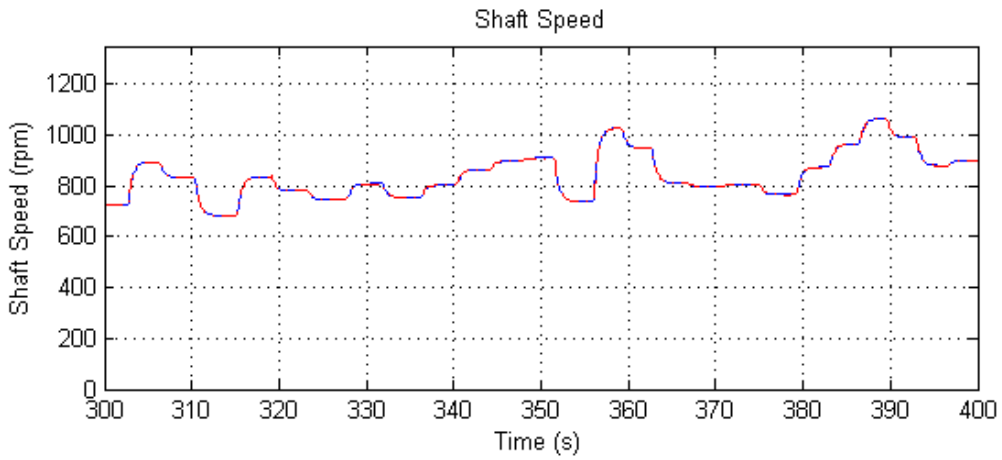

Figure 4.8: Shaft speed of the DC machine

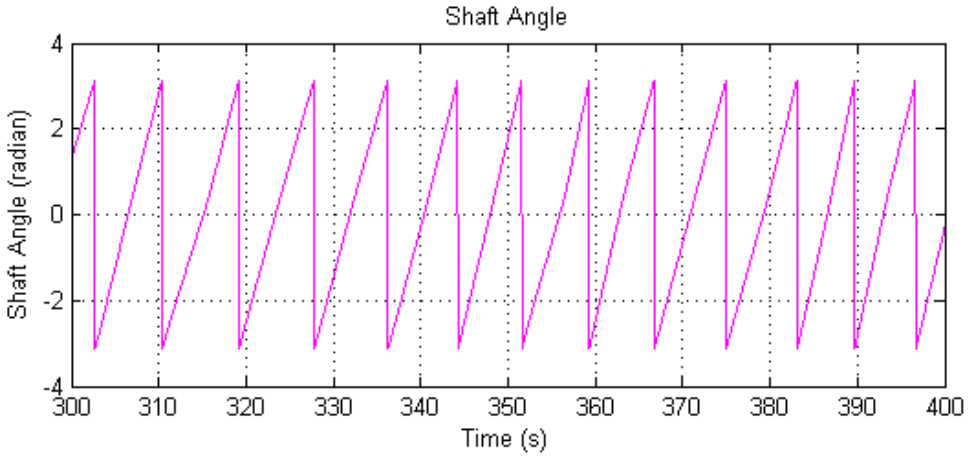

Figure 4.9: shaft angle of the DC machine

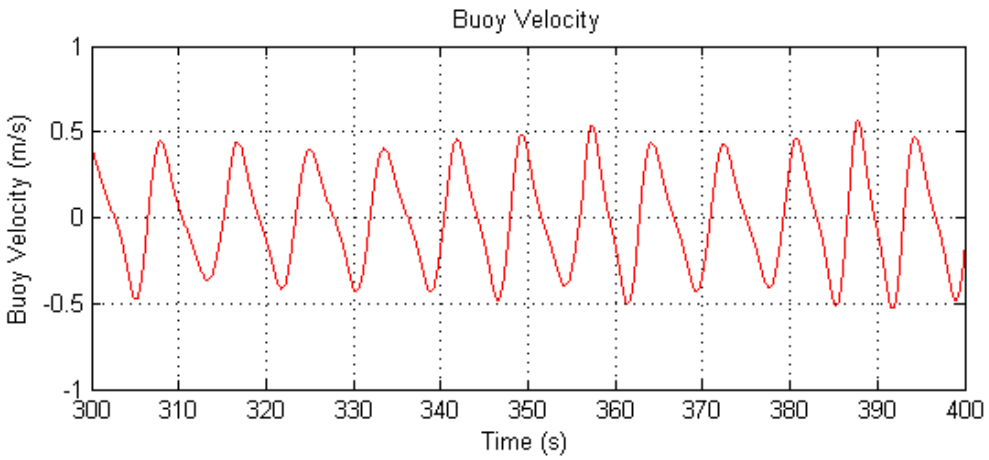

Figure 4.10: Buoy velocity

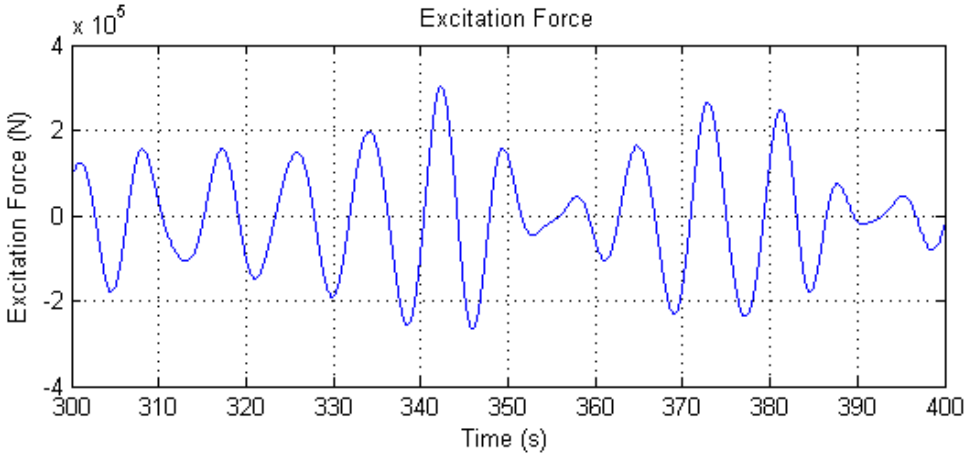

Figure 4.11: Wave excitation force

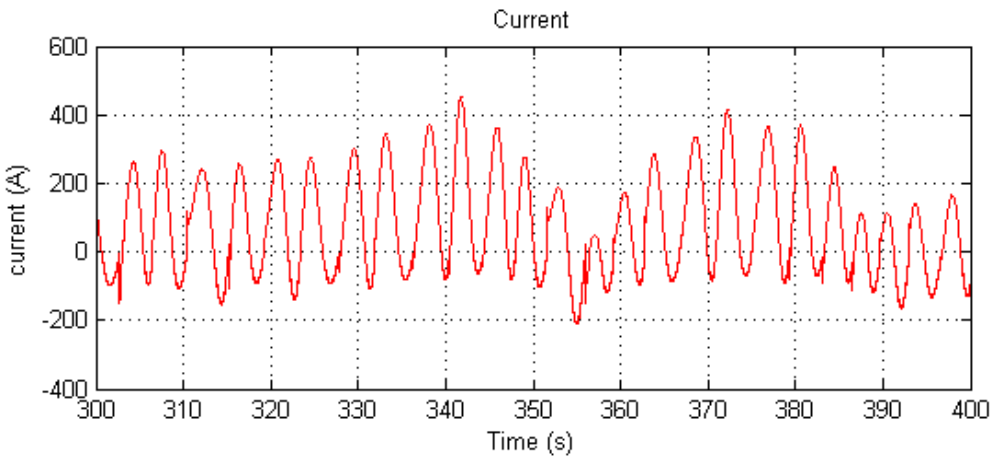

Figure 4.12: Output current of the generator

4.4.3 Energy Extraction with Different Significant Wave Heights and Peak Periods

In order to validate that the system is able to work under different wave conditions, simulations of the system were carried out with irregular waves of four significant wave heights and five peak periods.

The significant wave heights in the simulations were chosen according to the equal energy transport theorem mentioned in Section 2.2.2, and the significant heights of 1.1314, 1.4142, 1.6971 and 1.9799 meters are equivalent to regular wave amplitudes of 0.4, 0.5, 0.6, 0.7 meters, respectively.

All of these waves were generated with the JONSWAP spectrum and random number generator; each case is different from another. In order to obtain a more accurate result, four cases of simulations were done for each significant wave height and peak period, each case running for 500 seconds, and then an average value was calculated. The average values are provided in Table 4.14. Results from the 80 simulation cases validate that the system is able to work under a variety of irregular wave conditions and produce reasonable amounts of energy in comparison to the previous research with similar PTO conditions [29, 34]. The results of the 80 simulations are available in Appendix A.1.

Table 4.14: Average Electrical Power Production (kW) with a DC Machine at Different Significant Wave Heights and Peak Periods

H_{m0}(m) \ T_p(s)	6	7	8	9	10
1.1314	6.16	10.12	17.32	18.47	16.69
1.4142	12.22	19.23	21.37	21.57	20.78
1.6971	15.23	21.38	26.34	26.40	26.24
1.9799	24.00	31.65	33.09	33.85	29.49

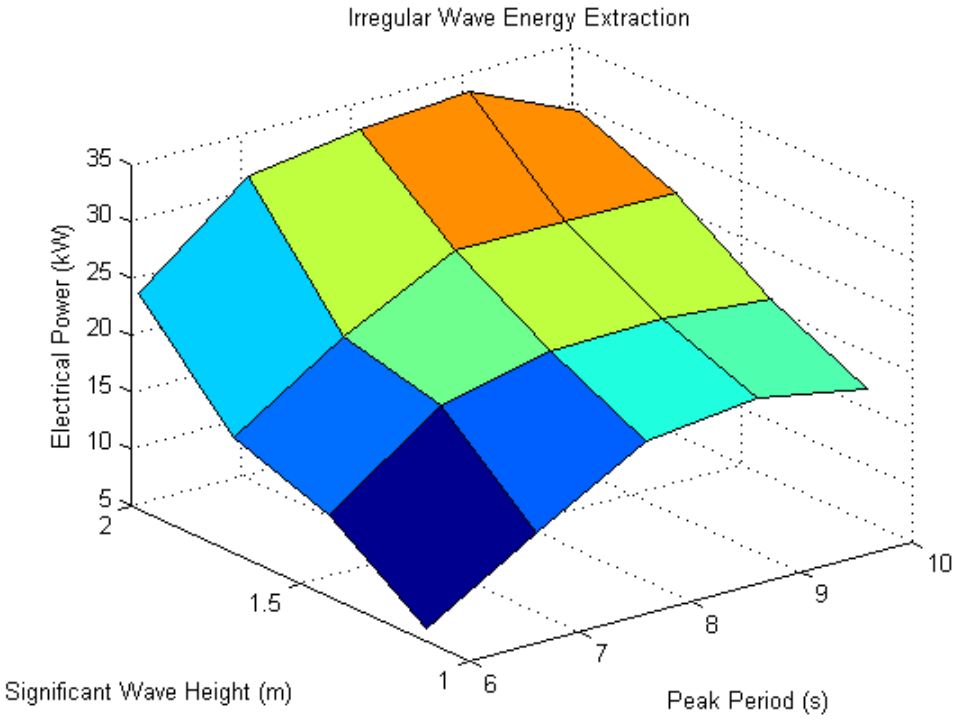

Figure 4.13: Electrical power production with a DC machine and irregular waves

From the data in Table 4.15, it can be observed that the energy extraction in accordance with significant wave height and peak period shows a similar trend as that under regular wave conditions as listed in [23]. In general, energy extraction increases as the significant wave height becomes larger; however, it does not necessarily increase as the peak period increases, although theoretically waves with a large period contain more energy. From Table 4.15, it can be seen that the maximum electrical power production tends to appear at

a peak period of 9 seconds. According to the electrical power matrix in [3], the most power should be produced at an energy period (T_e) of 8.5 seconds. With the parameters used in this study, T_e can be calculated with the following equations [37, 38]:

$$m_{-1} = \frac{1}{16} H_{m0}^2 \omega \frac{4.2+\gamma}{5+\gamma} \tag{4.11}$$

$$m_0 = \frac{1}{16} H_{m0}^2 \tag{4.12}$$

$$T_e = 2\pi \frac{m_{-1}}{m_0} = T_p \frac{4.2+\gamma}{5+\gamma} \tag{4.13}$$

When $T_p = 9s$, $T_e \approx 8.35s$, and it is very close to $8.5s$. Thus, the changes of electrical power production in accordance with significant wave height and energy period match quite well with the results in [3].

A 3-D plot of the data is given in Figure 4.13, in order to provide an intuitive illustration of the data in Table 4.15. Results from the 80 simulation cases validate that the system is able to work under a variety of irregular wave conditions and produce reasonable amounts of energy.

4.5 WEC Model with an AC Synchronous Machine under Irregular Wave Conditions

4.5.1 Simulation Setup

In simulations of this study, parameters in Table 4.9 and 4.10 were adopted; but wave amplitude and period, buoy size and PTOS gear ratio varied in different cases of simulations and these parameters would be specified for each case.

Simulation results are shown in the following steps. First, a simulation example with commonly used parameters is given in the next section. Energy extraction results and system-steady operation waveforms are provided to verify its feasibility and suboptimal nature. Second, energy extraction from waves with different amplitudes and periods are obtained, validating that the system is suitable for waves with a wide range of amplitudes and periods.

4.5.2 A Simulation Example

To show the details of the systems performance, a simulation example is provided as follows. In this simulation example, the significant wave height of the irregular wave is 1.4142 meters and the peak period is 8 seconds, and the simulation is run for 250 seconds. In this case, the average electrical power production is 33.0276 kW during the 250-second period.

The wave elevation in this simulation example from the 100th second to the 250th second is shown in Figure 4.6, and the cumulative energy production during this period is shown in Figure 4.15. It can be seen that energy extraction generally increases as time elapses, although the power can be very different at different points of time because of the irregular wave elevations. This proves that the system produces more energy than it consumes.

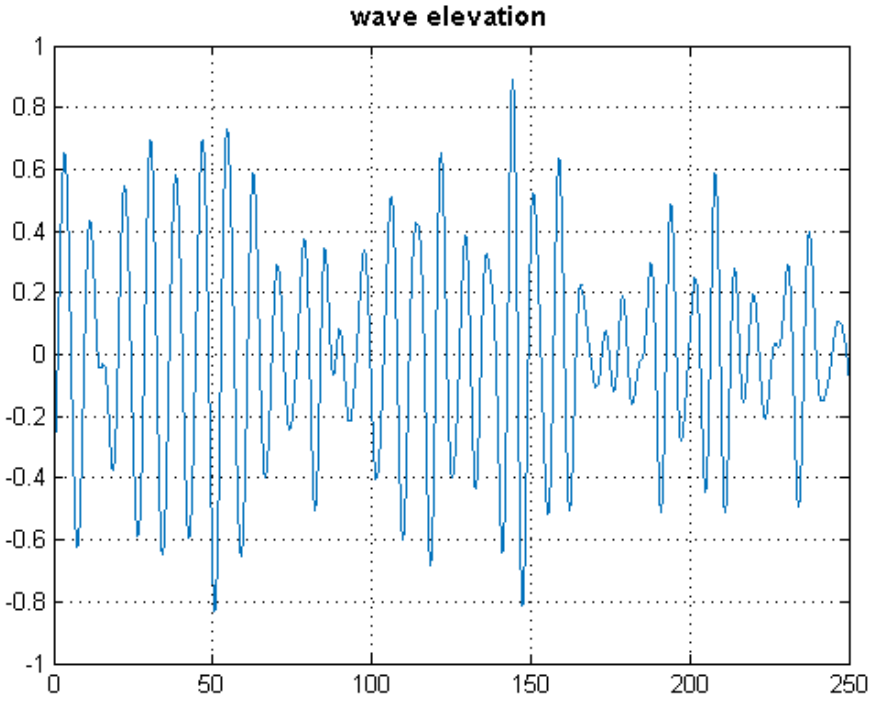

Figure 4.14: Wave elevation

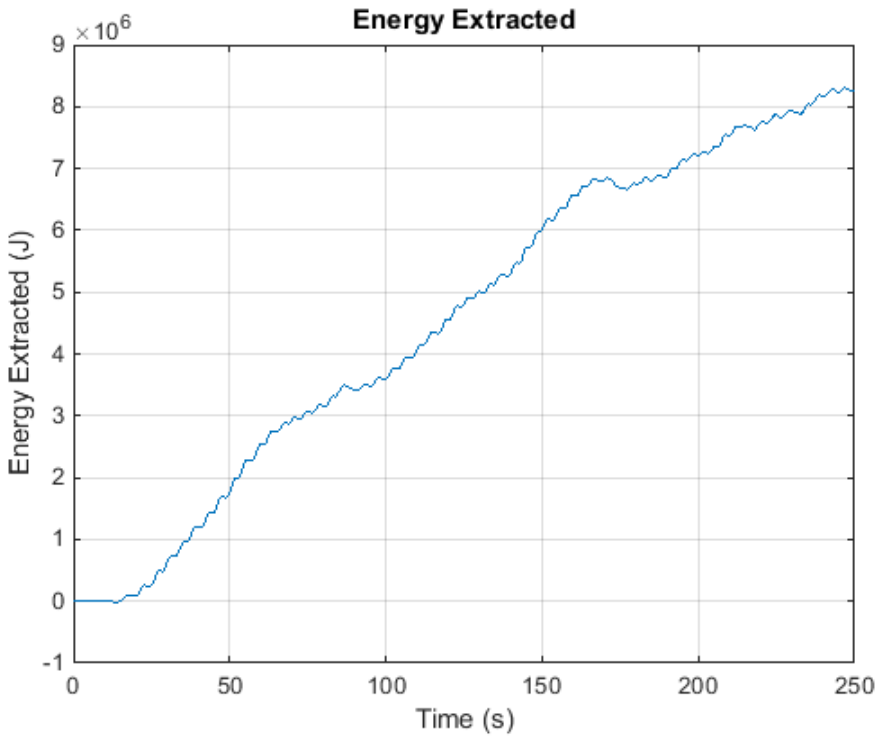

Figure 4.15: Cumulative electrical energy production with an AC machine and irregular wave

In order to reveal details of system operation, detailed operation data from the 100th second to the 200th second are shown in the following figures. The generator shaft speed is shown in Figure 4.16. The blue curve is the shaft speed reference and the red curve is the actual generator shaft speed in the simulation. It can be seen from the figure that the control algorithm effectively maintained the generator speed consistent with its reference. Figure 4.17 shows the shaft angle of the generator, Figure 4.18 shows the buoy velocity, and Figure 4.19 shows the wave excitation force; from the three plots, it can be observed that shaft angle of the generator and buoy velocity are kept in resonance with the excitation force. The PTO force is shown in Figure 4.20. The DC bus voltage is shown in Figure 4.21 and it can be seen that the voltage is maintained quite stable and the the fluctuation is moderate. The electromagnetic torque of the generator is shown in Figure 4.22. Positive torque means the machine is working in generator mode, while negative torque means it is working in motor mode. From the plot, it can be seen that the machine works in generator mode most of

the time, but it needs to work in motor mode to maintain the electric machine rotating in resonance with wave excitation force.

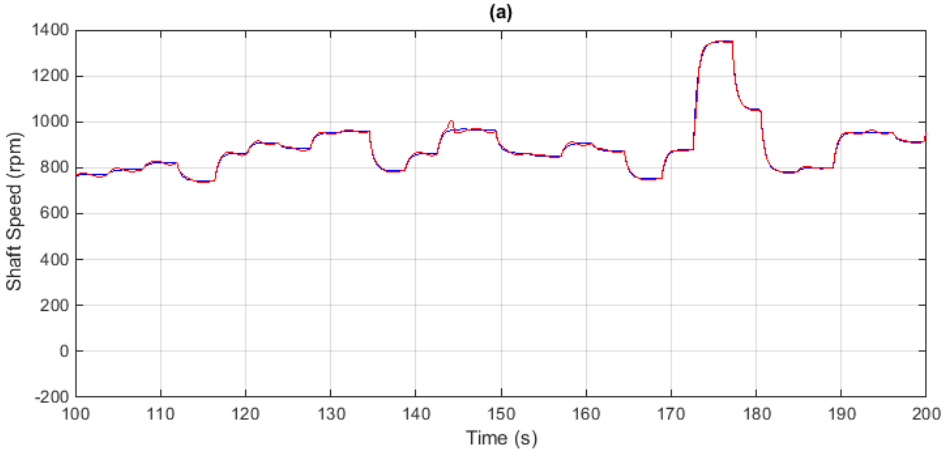

Figure 4.16: Shaft speed of the AC machine

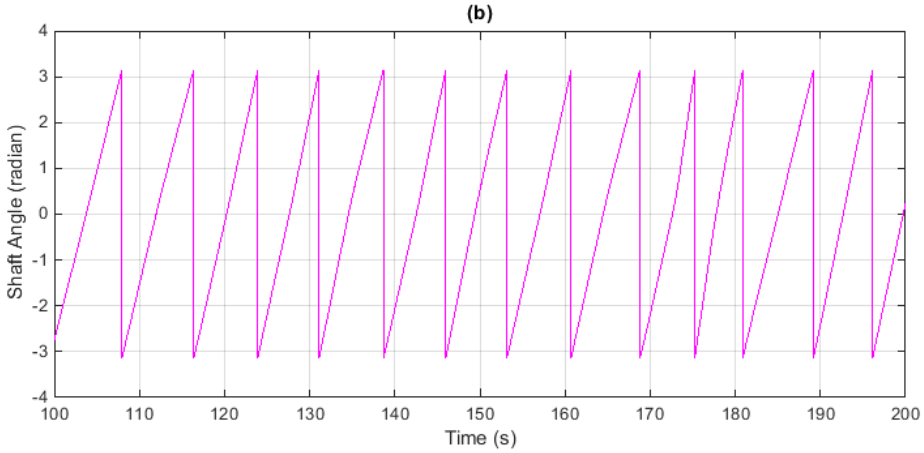

Figure 4.17: shaft angle of the AC machine

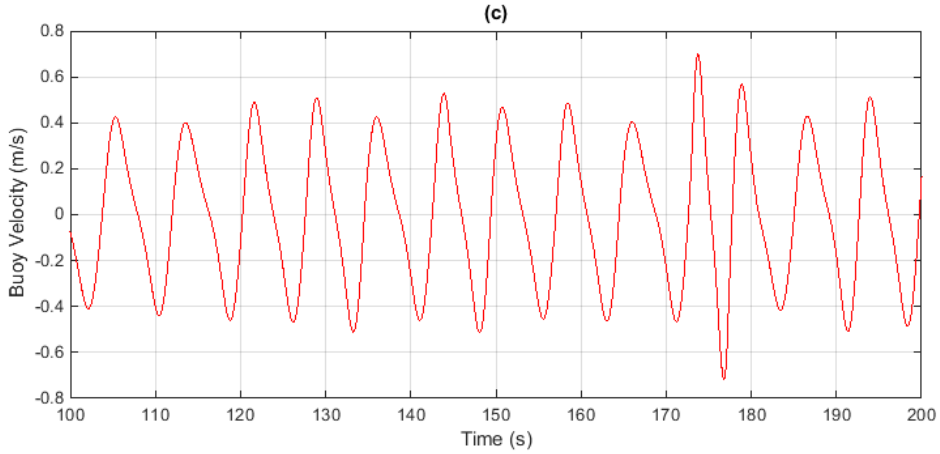

Figure 4.18: Buoy velocity

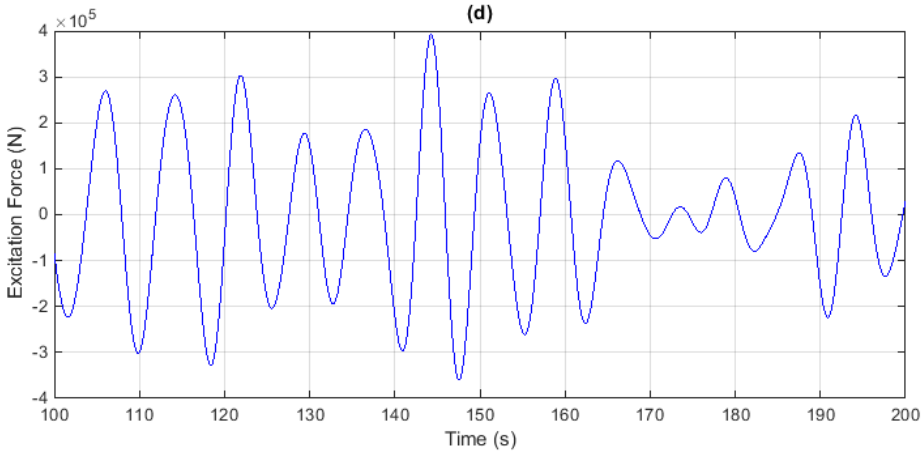

Figure 4.19: Wave excitation force

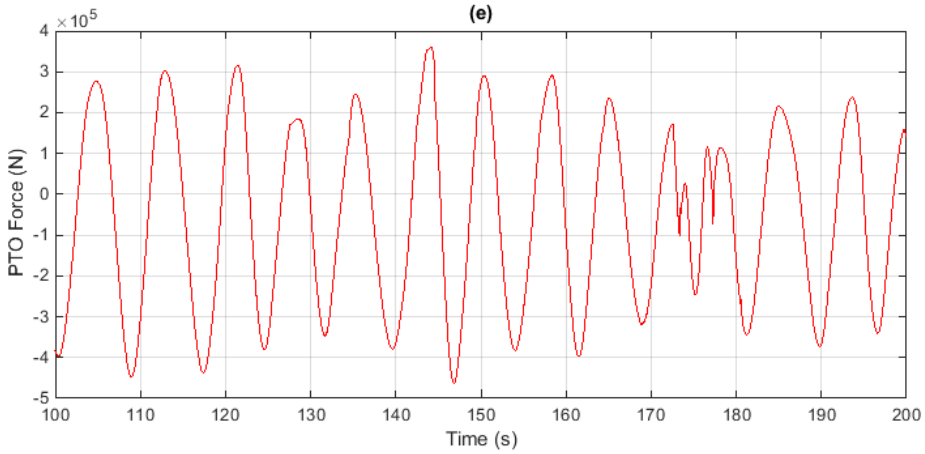

Figure 4.20: PTO force

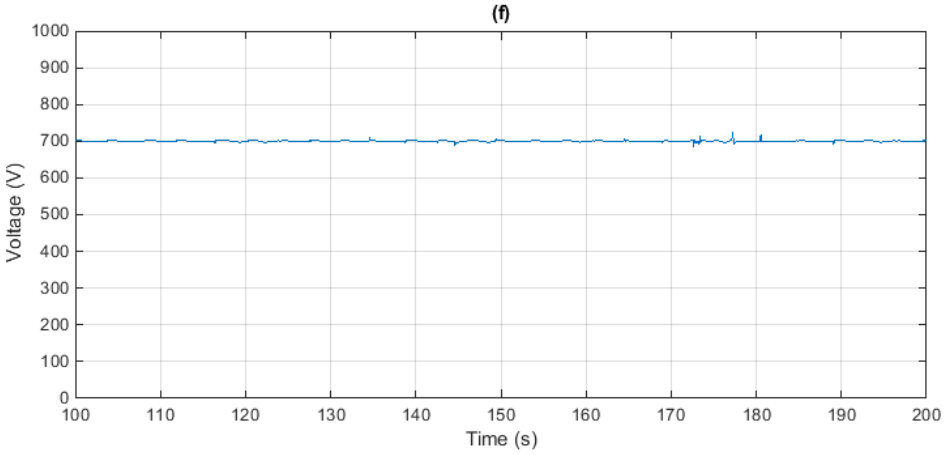

Figure 4.21: DC bus voltage

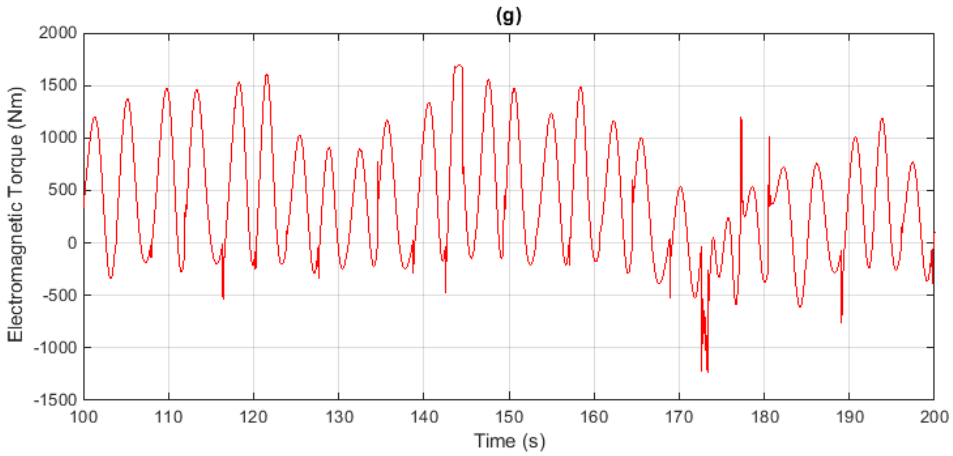

Figure 4.22: Electromagnetic torque of the generator

4.5.3 The Influence of Significant Wave Height and Peak Period

In order to validate the system is able to work under different wave conditions, waves with different significant wave heights and peak periods need to be tested. In this study, 160 simulations were carried out and each ran for 250 seconds - 8 simulations were carried out at each of the 4 significant wave heights and 5 peak periods. Table 4.15 provides the average values of electrical power production at different significant wave heights and peak periods, with a buoy radius of 5 meters, gear ratio of 110, and the generators moment of inertia of 15 $kg \cdot m^2$. In Table 4.15, H_{m0} is significant wave height, and T_p is peak period. The results of the 160 simulations are available in Appendix A.2.

Table 4.15: Average Electrical Power Production (kW) with an AC Machine at Different Significant Wave Heights and Peak Periods

H_{m0}(m) \ T_p(s)	6	7	8	9	10
1.1314	16.45	22.68	26.72	28.50	26.81
1.4142	25.41	33.94	37.23	37.29	35.44
1.6971	30.69	38.22	44.76	42.74	40.58
1.9799	42.09	50.14	52.13	45.68	42.98

A 3-D plot of the data is given in Figure 4.23, in order to provide an intuitive illustration of the data in Table 4.15. Results from the 160 simulation cases validate that the

system is able to work under a variety of irregular wave conditions and produce reasonable amounts of energy.

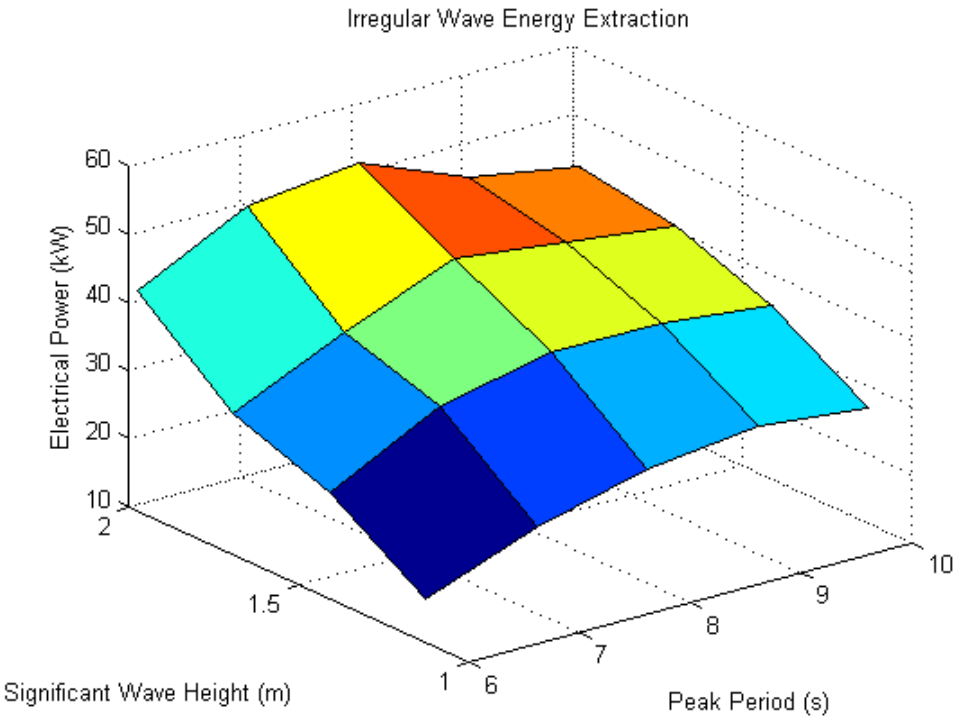

Figure 4.23: Electrical power production with an AC machine and irregular waves

CHAPTER 5: CONCLUSION AND FUTURE WORK

This thesis introduced a novel slider crank WEC, and proposed a nonparametric control method for the system. The control method keeps the generator rotate in resonance with wave excitation force and enables the system to achieve a suboptimal energy extraction.

For the hydrodynamics part, frequency domain hydrodynamics analysis was applied at first for the simplicity of the modeling and then time-domain hydrodynamics analysis was applied to handle nonlinearity of PTO. Wave excitation forces are calculated separately for regular waves and irregular waves.

For the evaluation of the system and the control method, four conditions have been considered, namely the WEC with a DC machine under regular wave conditions, the WEC with a AC synchronous machine under regular wave conditions, the WEC with a DC machine under irregular wave conditions, and the WEC with a AC synchronous machine under irregular wave conditions. A Matlab/Simulink model was built and a large number of simulations were carried out under each condition. Simulation results show that a suboptimal energy extraction can be achieved under the four conditions with a variety of wave amplitudes/significant wave heights and periods/peak periods, and AC synchronous machine had a better performance than the DC machine. The AC synchronous machine does not only have a higher efficiency, but also increases system stability and reduces the influence on energy extraction imposed by gear ratio and inertia.

Future work of this study includes analysis of the system with modified slider crank parameters, a more efficient variable speed AC machine and drives, as well as predictors for wave excitation force.

BIBLIOGRAPHY

[1] National Oceanic and Atmospheric Administration, "Ocean," `http://www.noaa.gov/ocean.html`, 2015 (accessed March 22, 2015).

[2] T. Brekken, "Fundamentals of ocean wave energy conversion, modeling, and control," in *Proc. IEEE International Symposium on Industrial Electronics (ISIE)*, Bari, Italy, July 4-7 2010, pp. 3921–3966.

[3] V. S. Neary et al, *Methodology for design and economic analysis of Marine Energy Conversion (MEC) technologies*, Sandia National Laboratories, Albuquerque, NM, 2014.

[4] European Commission, "Ocean energy conversion in europe, recent advancements and prospects, center for renewable energy sources," `http://wavec.org/client/files/OceanEnergyConversionEurope_CRES.pdf`, 2006.

[5] T.K.A. Brekken, B.A. Batten, and E.A. Amon, "From blue to green [ask the experts]," *Control Systems, IEEE*, vol. 31, no. 5, pp. 18–24, October 2011.

[6] Zhen Liu, Beom-Soo Hyun, Jiyuan Jin, Yonghyeon Choi, Hongda Shi, and Qin Zhang, "A wave focusing device for owc wave energy convertor," in *OCEANS 2010 IEEE - Sydney*, May 2010, pp. 1–5.

[7] M. Trapanese, "Optimized design of a sea wave energy conversion system," in *Industrial Electronics, 2008. IECON 2008. 34th Annual Conference of IEEE*, Nov 2008, pp. 2051–2054.

[8] N.M. Kimoulakis and A.G. Kladas, "Modeling and control of a coupled electromechanical system exploiting heave motion, for energy conversion from sea waves," in *Power Electronics Specialists Conference, 2008. PESC 2008. IEEE*, June 2008, pp. 3850–3853.

[9] N.M. Kimoulakis, A.G. Kladas, and J.A. Tegopoulos, "Cogging force minimization in a coupled permanent magnet linear generator for sea wave energy extraction applications," *Magnetics, IEEE Transactions on*, vol. 45, no. 3, pp. 1246–1249, March 2009.

[10] H. Polinder, B.C. Mecrow, A.G. Jack, P.G. Dickinson, and M.A. Mueller, "Conventional and tfpm linear generators for direct-drive wave energy conversion," *Energy Conversion, IEEE Transactions on*, vol. 20, no. 2, pp. 260–267, June 2005.

[11] T.K.A. Brekken, H.M. Hapke, C. Stillinger, and J. Prudell, "Machines and drives comparison for low-power renewable energy and oscillating applications," *Energy Conversion, IEEE Transactions on*, vol. 25, no. 4, pp. 1162–1170, Dec 2010.

[12] J.F. Chozas and H.C. Soerensen, "State of the art of wave energy in spain," in *Electrical Power Energy Conference (EPEC), 2009 IEEE*, Oct 2009, pp. 1–6.

[13] Oahu Hawaii Ocean Power Technologies, Kaneohe Bay, "Project at marine corps base hawaii (mcbh)," `http://www.oceanpowertechnologies.com/projects.htm`, accessed 11/12/2010.

[14] Pelamis Wave Power, "Project overview," `Availableathttp://www.pelamiswave.com/our-projects/project-overview`, accessed 11/12/2010.

[15] The European Marine Energy Centre Ltd. EMEC Orkney, "Wave energy developers," `http://www.emec.org.uk/wave_energy_developers.asp`, accessed 11/12/2010.

[16] K.K. Ahn, D.Q. Truong, Hoang Huu Tien, and Jong Il Yoon, "An innovative design of wave energy converter," *Renewable Energy*, vol. 42, pp. 186–194, 2012.

[17] H.B. Karayaka, H. Mahlke, D. Bogucki, and M. Mehrubeoglu, "A rotational wave energy conversion system development and validation with real ocean wave data," in *Power and Energy Society General Meeting, 2011 IEEE*, July 2011, pp. 1–7.

[18] K. Rhinefrank, A. Schacher, J. Prudell, T.K.A. Brekken, C. Stillinger, J.Z. Yen, S.G. Ernst, A. von Jouanne, E. Amon, R. Paasch, A. Brown, and A. Yokochi, "Comparison of direct-drive power takeoff systems for ocean wave energy applications," *Oceanic Engineering, IEEE Journal of*, vol. 37, no. 1, pp. 35–44, Jan 2012.

[19] J. Hals, T. Bjarte-Larsson, and J. Falnes, "Optimum reactive control and control by latching of a wave-absorbing semisubmerged heaving sphere," in *Proc. 21st Int. Conf. Offshore Mech. Artic Eng.*, Oslo, Norway, Jun. 2328 2002, pp. 1–9.

[20] Rafael Frankel, "The olynthus mill, its origin, and diffusion: Typology and distribution," *American Journal of Archaeology*, vol. 107, no. 1, pp. pp. 1–21, 2003.

[21] Tullia Ritti, Klaus Grewe, and Paul Kessener, "A relief of a water-powered stone saw mill on a sarcophagus at hierapolis and its implications," *Journal of Roman Archaeology*, vol. 20, pp. 139–163, 1 2007.

[22] Adam Robert Lucas, "Industrial milling in the ancient and medieval worlds: A survey of the evidence for an industrial revolution in medieval europe," *Technology and Culture*, vol. 46, no. 1, pp. pp. 1–30, 2005.

[23] Yuanrui Sang, H. Bora Karayaka, Yanjun Yan, and J.Z. Zhang, "Resonance control strategy for a slider crank wec power take-off system," in *Oceans - St. John's, 2014*, Sept 2014, pp. 1–8.

[24] M. Njeh, S. Cauet, P. Coirault, and P. Martin, "Torque harmonic reduction in hybrid vehicles," in *American Control Conference (ACC), 2010*, June 2010, pp. 5838–5843.

[25] Johannes Falnes, *Ocean waves and oscillating systems: linear interactions including wave-energy extraction*, Cambridge university press, 2002.

[26] A. Hulme, "The wave forces acting on a floating hemisphere undergoing forced periodic oscillations," *Journal of Fluid Mechanics*, vol. 121, pp. 443–463, 8 1982.

[27] National Renewable Energy Laboratory and Sandia Corporation, "Wec-sim user manual," http://prod-http-80-800498448.us-east-1.elb.amazonaws.com/w/images/c/c7/WEC_Sim_User_Manual_v1.0.pdf, accessed 12/20/2014.

[28] K. Hasselman et al, "Measurements of wind-wave growth and swell decay during the joint north sea wave project (jonswap)," Tech. Rep., Deutches Hydrographisches Institut, 1973.

[29] E. Tedeschi, M. Carraro, M. Molinas, and P. Mattavelli, "Effect of control strategies and power take-off efficiency on the power capture from sea waves," *Energy Conversion, IEEE Transactions on*, vol. 26, no. 4, pp. 1088–1098, Dec 2011.

[30] Hakan Yavuz, "On control of a pitching and surging wave energy converter," *International Journal of Green Energy*, vol. 8, no. 5, pp. 555–584, 2011.

[31] A. Kyllingstad, "Approximate analysis concerning wave-power absorption by hydrodynamically interacting buoys," 1982.

[32] W.E. Cummins, "The impulse response function and ship motions," Tech. Rep., Schiffstechnik, 1962.

[33] N. Yilmaz H. Karayaka, D. Souders, "A cfd based 2-d validation study of the dynamics of a semi-submerged sphere in heave motion," in *IX. Clean Energy Symposium, UTES13*, Konya, Turkey, December 2013.

[34] E. Tedeschi and M. Molinas, "Tunable control strategy for wave energy converters with limited power takeoff rating," *Industrial Electronics, IEEE Transactions on*, vol. 59, no. 10, pp. 3838–3846, Oct 2012.

[35] Jørgen Hals, Johannes Falnes, and Torgeir Moan, "Constrained optimal control of a heaving buoy wave-energy converter," *Journal of Offshore Mechanics and Arctic Engineering*, vol. 133, no. 1, pp. 011401, 2011.

[36] M Lawson, YH Yu, A Nelessen, K Ruehl, and C Michelen, "Implementing nonlinear buoyancy and excitation forces in the wec-sim wave energy converter modeling tool: Preprint," Tech. Rep., National Renewable Energy Laboratory (NREL), Golden, CO., 2014.

[37] Det Norske Veritas, "Modelling and analysis of marine operations," *Oslo, Norway*, 2011.

[38] B. Cahill, "Wave period ratios and the calculation of wave power," in *Proc. the 2nd Marine Energy Technology Symposium, METS2014*, Seattle, WA, 2014, pp. 1–10.

Appendices

APPENDIX A: IRREGULAR WAVE ENERGY EXTRACTION DATA

A.1 Irregular Wave Energy Extraction with a DC Machine

Table A.1: Average Electrical Power Production (kW) with a DC Machine at Different Significant Wave Heights and Peak Periods (Group 1)

H_{m0}(m) \ T_p(s)	6	7	8	9	10
1.1314	4.3970	4.8885	16.3675	16.8732	19.1713
1.4142	13.9300	20.6458	22.9938	24.4423	15.5145
1.6971	15.9642	19.3985	22.2265	29.2240	27.2883
1.9799	26.7288	33.7938	26.1765	39.1773	27.1640

Table A.2: Average Electrical Power Production (kW) with a DC Machine at Different Significant Wave Heights and Peak Periods (Group 2)

H_{m0}(m) \ T_p(s)	6	7	8	9	10
1.1314	6.9909	9.3500	20.1973	19.5015	16.1488
1.4142	11.6620	15.7253	19.1705	19.9620	22.7938
1.6971	16.5635	17.4918	22.1635	27.5573	24.6258
1.9799	21.0263	33.5073	38.1638	32.5828	30.5030

Table A.3: Average Electrical Power Production (kW) with a DC Machine at Different Significant Wave Heights and Peak Periods (Group 3)

H_{m0}(m) \ T_p(s)	6	7	8	9	10
1.1314	8.3670	12.4033	16.3610	18.5388	16.7665
1.4142	12.7580	19.9090	21.6575	18.5203	22.2115
1.6971	14.9423	27.8030	28.6553	25.5185	24.1135
1.9799	18.0918	31.2870	36.3030	32.9173	30.7260

Table A.4: Average Electrical Power Production (kW) with a DC Machine at Different Significant Wave Heights and Peak Periods (Group 4)

H_{m0}(m) \ T_p(s)	6	7	8	9	10
1.1314	4.8855	13.8510	16.3675	18.9678	14.6880
1.4142	10.5483	20.6455	21.6710	23.3550	22.5833
1.6971	13.4395	20.8405	32.3038	23.2995	28.9260
1.9799	30.1725	27.9930	31.7065	30.7278	29.5678

A.2 Irregular Wave Energy Extraction with an AC Machine

Table A.5: Average Electrical Power Production (kW) with an AC Machine at Different Significant Wave Heights and Peak Periods (Group 1)

H_{m0}(m) \ T_p(s)	6	7	8	9	10
1.1314	16.6324	25.4256	25.0112	29.0724	28.1176
1.4142	23.9484	38.2888	38.8148	37.8208	36.0572
1.6971	29.3512	38.3840	48.4640	36.6968	41.8120
1.9799	38.6284	46.1280	50.8000	47.2000	44.3760

Table A.6: Average Electrical Power Production (kW) with an AC Machine at Different Significant Wave Heights and Peak Periods (Group 2)

H_{m0}(m) \ T_p(s)	6	7	8	9	10
1.1314	14.9192	23.4896	29.5340	30.7748	23.3332
1.4142	22.1324	36.5576	33.4142	37.8208	37.3820
1.6971	31.2704	43.6320	41.3480	41.1480	42.2240
1.9799	41.2720	52.4360	45.7240	42.8400	41.5440

Table A.7: Average Electrical Power Production (kW) with an AC Machine at Different Significant Wave Heights and Peak Periods (Group 3)

H_{m0}(m) \ T_p(s)	6	7	8	9	10
1.1314	15.5345	20.0848	30.7704	31.2932	28.3936
1.4142	30.9660	36.1332	35.3444	34.1444	29.0548
1.6971	21.4976	36.0432	44.5240	45.7600	41.9200
1.9799	41.2720	53.0800	49.3960	50.1080	42.1560

Table A.8: Average Electrical Power Production (kW) with an AC Machine at Different Significant Wave Heights and Peak Periods (Group 4)

H_{m0}(m) \ T_p(s)	6	7	8	9	10
1.1314	16.6859	23.1568	25.7208	25.7596	27.886
1.4142	27.0888	39.4316	40.1080	37.4852	36.4628
1.6971	33.2208	34.9652	41.1400	45.3080	36.6356
1.9799	36.5820	51.7880	52.8160	46.6600	43.8960

Table A.9: Average Electrical Power Production (kW) with an AC Machine at Different Significant Wave Heights and Peak Periods (Group 5)

H_{m0}(m) \ T_p(s)	6	7	8	9	10
1.1314	17.2328	23.1568	24.9004	29.0724	26.9300
1.4142	27.8244	28.1288	33.8076	33.5984	35.7584
1.6971	34.2644	43.6320	53.5120	45.3080	44.0240
1.9799	43.7240	43.5440	55.8560	46.6600	44.3760

Table A.10: Average Electrical Power Production (kW) with an AC Machine at Different Significant Wave Heights and Peak Periods (Group 6)

H_{m0}(m) \ T_p(s)	6	7	8	9	10
1.1314	14.9192	23.4940	26.9916	30.7748	27.8316
1.4142	23.9540	27.6140	43.2160	38.8136	36.9300
1.6971	32.7068	38.7084	48.9000	36.8636	35.7348
1.9799	47.0360	40.1680	58.5520	47.2000	41.5440

Table A.11: Average Electrical Power Production (kW) with an AC Machine at Different Significant Wave Heights and Peak Periods (Group 7)

H_{m0}(m) \ T_p(s)	6	7	8	9	10
1.1314	16.6324	22.1936	25.8772	27.3556	26.6160
1.4142	22.1328	30.9396	40.0920	43.4200	38.0728
1.6971	22.5220	37.5360	41.8160	42.2920	40.0760
1.9799	44.1840	54.9560	55.7080	42.8400	41.5440

Table A.12: Average Electrical Power Production (kW) with an AC Machine at Different Significant Wave Heights and Peak Periods (Group 8)

H_{m0}(m) \ T_p(s)	6	7	8	9	10
1.1314	19.0160	20.4724	24.9528	23.8812	25.3444
1.4142	25.2104	34.4556	33.0276	35.2352	33.8032
1.6971	40.6920	32.8656	38.3880	48.5200	42.2240
1.9799	44.0600	59.0080	48.1608	41.9680	44.3760

APPENDIX B: SOURCE CODE

B.1 Wave Exciation Force Calculation for Regular Wave with Frequency-domain Hydrodynamics and a DC Machine

B.1.1 Main Code

```
clear;clc;close all;

%=========================================================================%
%==========================Initialization=================================%
% initial inertia: 10
% initial viscous friction coefficient: 0.32

%Callback for the simulink model
Ts=20e-6; % Sampling time

%%% setting 1 %%%
gr=115;    % Gear ratio
%======================
aa=20e-6/(.5+20e-6);


%Hydrodynamics initialization
Start_Time=0;              % time start
End_Time=100;              % final time
Interval=0.01;             % simpling time interval
rho=1020;                  % the density of water
g=9.81;                    % acceleration of gravity

%%% setting 2 %%%
a=5;%0.9533;                  % buoy radius
%======================
Rv=10;                  % Viscous force coefficient
Rf=0;                      % Friction force coefficient

%omega=1;                   % The angular velocity of water wave

%%% setting 3 %%%
A=0.5;                     % The maximum amplitude of water wave, ...
   initialized again in the slider crank function.
%======================
%%% setting 4 %%%
f=1/6;                      % The frequency of water wave
%======================
omega=2*pi*f;              % The angular velocity of water wave
k=omega^2/g;               % Wave number for infinite water depth
Kaq=k*a;                   % ka
```

```
zw=@(t)A*sin(omega*t+0.2493);    % the function of water wave

%Slider-Crank initialization
r=0.5;                      % Radius of crank. used again in the rk4sys_step ...
   function and slider crank function.
l=1;                        % Length of rod, used again in the slider crank ...
   function.
lambda=r/l;                 % used again in the slider crank function.
B=0.01;                    % Viscous friction, used again in the slider ...
   crank function.
J=10;                      % inertia of flywheel, used again in the slider ...
   crank function.
dr=1;                      % (Used to be r+A) Distance between the lowest ...
   edge of the crank and the reference water surface
mcrp=10;                   % Total of mass of piston (or slider) and ...
   connecting rod respectively.

Fu=zeros(1,(End_Time-Start_Time)/Interval+1);

%Generator initialization
L_af = 1.234; % Mutual inductance between the field and the rotating ...
   armature coils.
V_f = 220; % Field voltage.
r_f = 150; % Resistance of field windings
I_f = V_f/r_f; % Current of field windings
L_aa = 0.016; % Self-inductance of the field and armature windings.
r_a = 0.78;  % Resistance of the armature coils.
kv = L_af*I_f; % Stator constant

%=========================================================================%
%===Calculating mu, epsilon and kappa through graphical observation======%

Ka=[0 0.05 0.1 0.2 0.3 0.4 0.5 0.6 0.7 0.8 0.9 1.0 1.2 1.4 1.6 1.8 2.0 2.5 ...
   3.0 4.0 5.0 6.0 7.0 8.0 9.0 10.0]';
Amass=[0.8310 0.8764 0.8627 0.7938 0.7157 0.6452 0.5861 0.5381 0.4999 ...
   0.4698 0.4464 0.4284 0.4047 0.3924 0.3871 0.3864 0.3884 0.3988 0.4111 ...
   0.4322 0.4471 0.4574 0.4647 0.4700 0.4740 0.4771]';
Damping=[0 0.1036 0.1816 0.2793 0.3254 0.3410 0.3391 0.3271 0.3098 0.2899 ...
   0.2691 0.2484 0.2096 0.1756 0.1469 0.1229 0.1031 0.0674 0.0452 0.0219 ...
   0.0116 0.0066 0.0040 0.0026 0.0017 0.0012]';

kappa(1)=1;
for i=2:length(Ka)
    kappa(i)=sqrt(4*Damping(i)/(3*pi*Ka(i)));
end

Mu = interp1(Ka,Amass,Kaq','cubic');
Ep = interp1(Ka,Damping,Kaq','cubic');
kap= interp1(Ka,kappa,Kaq','cubic');

%=========================================================================%
%Calculating Coefficients of the Differential Equation of Buoy Displacement
```

```
Sb=rho*g*pi*a^2;%785890;
mm=rho*(2*pi/3)*a^3;
m=mm*(1+Mu);%267040+156940;
R=Rv+Rf+Ep*omega*mm;%91520;
Fe=@(t)kap*rho*g*pi*a^2*zw(t);
t = Start_Time:Interval:End_Time;
Ocean_Wave_AccP.signals.values=Fe(t)';
Ocean_Wave_AccP.time=t';

%Call to find initial angle
Initial_Angle_Solver;
```

B.1.2 Initial Angle Solver

```
% File name: Initial_Angle_Solver
format long;
f1=@(u)(dr-sqrt(l^2-(r*sin(u))^2))/r;
f2=@(u)cos(u);
u=0;
err=1;
while err>1e-12
    f1n=f1(u);
    f2n=f2(u);
    u=acos(f1n);
    err=abs(f1n-f2n);
end
disp('The Initial Angle is (in radian): ');
disp(u);
disp('In degrees: ');
disp(u/pi*180);
Theta_Initial=u;
```

B.1.3 Simulink Model

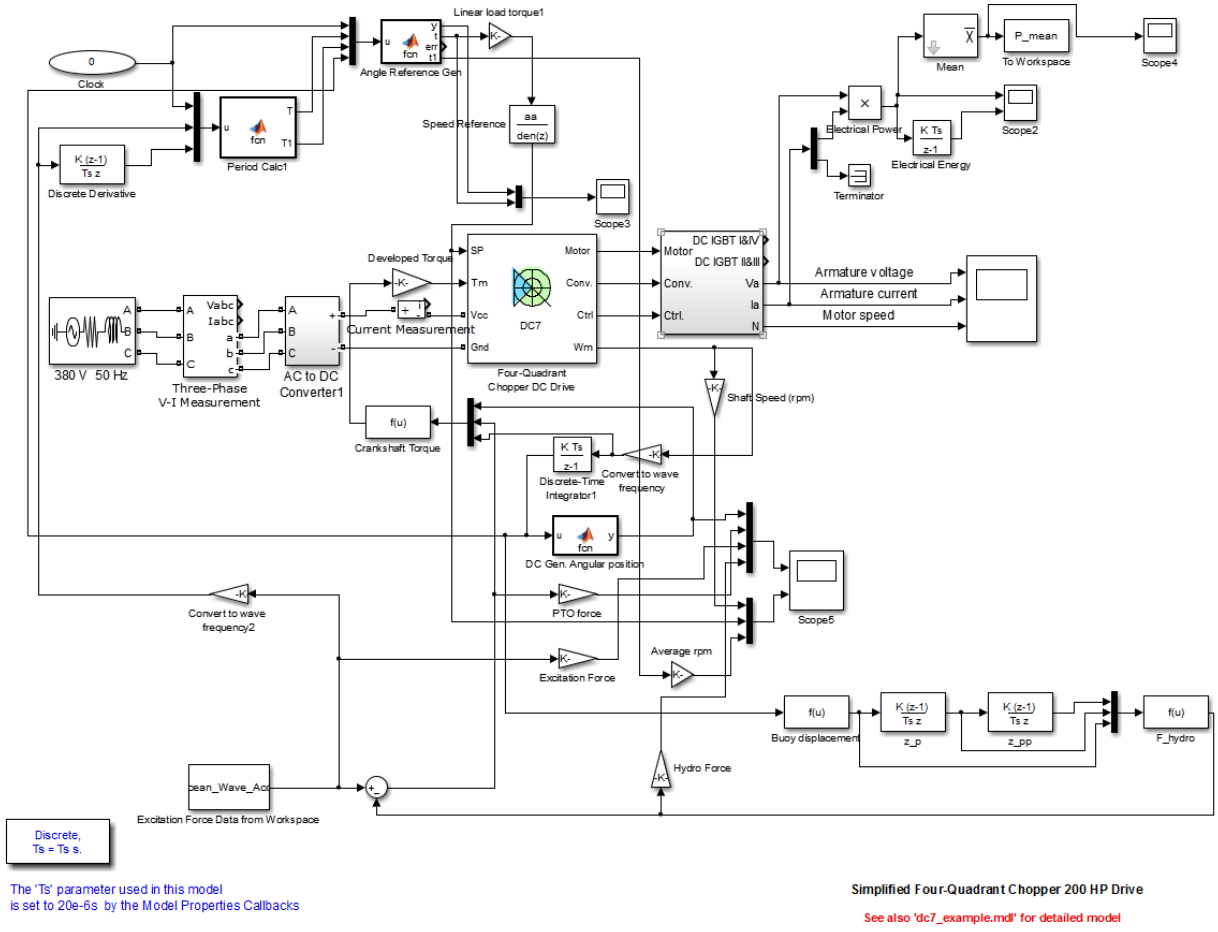

Figure B.1: Simulink model

B.2 Wave Exciation Force Calculation for Regular Wave with Time-domain Hydrodynamics Analysis and an AC Machine

B.2.1 Main Code

```
clear;clc;close all;

%=========================================================================%
%============================Initialization===============================%
% initial inertia: 10
% initial viscous friction coefficient: 0.32

%Callback for the simulink model
Ts=20e-6; % Sampling time
Td=1e-3; % Discrete Sampling time

%%% setting 1 %%%
```

```
gr=110;    % Gear ratio
%======================
aa=20e-6/(.5+20e-6);


%Hydrodynamics initialization
Start_Time=0;              % time start
End_Time=100;              % final time
Interval=0.01;             % simpling time interval
rho=1020;                  % the density of water
g=9.81;                    % acceleration of gravity

%%% setting 2 %%%
a=5;%0.9533;                  % buoy radius
%======================
Rv=10;                  % Viscous force coefficient
Rf=0;                      % Friction force coefficient

%omega=1;                   % The angular velocity of water wave

%%% setting 3 %%%
A=0.5;                     % The maximum amplitude of water wave, ...
   initialized again in the slider crank function.
%======================
%%% setting 4 %%%
f=1/6;                      % The frequency of water wave
%======================
omega=2*pi*f;              % The angular velocity of water wave
k=omega^2/g;               % Wave number for infinite water depth
Kaq=k*a;                   % ka

zw=@(t)A*sin(omega*t+0.2493);    % the function of water wave

%Slider-Crank initialization
r=0.5;                     % Radius of crank. used again in the rk4sys_step ...
   function and slider crank function.
l=1;                       % Length of rod, used again in the slider crank ...
   function.
lambda=r/l;                % used again in the slider crank function.
B=0.01;                   % Viscous friction, used again in the slider ...
   crank function.
J=10;                     % inertia of flywheel, used again in the slider ...
   crank function.
dr=1;                     % (Used to be r+A) Distance between the lowest ...
   edge of the crank and the reference water surface
mcrp=10;                  % Total of mass of piston (or slider) and ...
   connecting rod respectively.

Fu=zeros(1,(End_Time-Start_Time)/Interval+1);

%Generator initialization
L_af = 1.234; % Mutual inductance between the field and the rotating ...
   armature coils.
V_f = 220; % Field voltage.
```

```
r_f = 150; % Resistance of field windings
I_f = V_f/r_f; % Current of field windings
L_aa = 0.016; % Self-inductance of the field and armature windings.
r_a = 0.78;  % Resistance of the armature coils.
kv = L_af*I_f; % Stator constant

%=========================================================================%
%===Calculating mu, epsilon and kappa through graphical observation======%

Ka=[0 0.05 0.1 0.2 0.3 0.4 0.5 0.6 0.7 0.8 0.9 1.0 1.2 1.4 1.6 1.8 2.0 2.5 ...
    3.0 4.0 5.0 6.0 7.0 8.0 9.0 10.0]';
Amass=[0.8310 0.8764 0.8627 0.7938 0.7157 0.6452 0.5861 0.5381 0.4999 ...
    0.4698 0.4464 0.4284 0.4047 0.3924 0.3871 0.3864 0.3884 0.3988 0.4111 ...
    0.4322 0.4471 0.4574 0.4647 0.4700 0.4740 0.4771]';
Damping=[0 0.1036 0.1816 0.2793 0.3254 0.3410 0.3391 0.3271 0.3098 0.2899 ...
    0.2691 0.2484 0.2096 0.1756 0.1469 0.1229 0.1031 0.0674 0.0452 0.0219 ...
    0.0116 0.0066 0.0040 0.0026 0.0017 0.0012]';

kappa(1)=1;
for i=2:length(Ka)
    kappa(i)=sqrt(4*Damping(i)/(3*pi*Ka(i)));
end

Mu = interp1(Ka,Amass,Kaq','cubic');
Ep = interp1(Ka,Damping,Kaq','cubic');
kap= interp1(Ka,kappa,Kaq','cubic');

%=========================================================================%
%Calculating Coefficients of the Differential Equation of Buoy Displacement

Sb=rho*g*pi*a^2;%785890;
mm=rho*(2*pi/3)*a^3;
m=mm*(1+Mu);%267040+156940;
R=Rv+Rf+Ep*omega*mm;%91520;
Fe=@(t)kap*rho*g*pi*a^2*zw(t);
t = Start_Time:Interval:End_Time;
Ocean_Wave_AccP.signals.values=Fe(t)';
Ocean_Wave_AccP.time=t';
plot(Ocean_Wave_AccP.time,Ocean_Wave_AccP.signals.values)
%Call to find initial angle
Theta_Initial=Initial_Angle_Solver;
[bz,az]=RadiationKomega(a,Td);
Wave_Analysis;
```

B.2.2 Initial Angle Solver

```
% File name: Initial_Angle_Solver
function Theta_Initial=Initial_Angle_Solver()
format long;
%=========================================================================%
%Slider-Crank initialization
r=0.5;                    % Radius of crank. used again in the rk4sys_step ...
```

```
    function and slider crank function.
l=1;                        % Length of rod, used again in the slider crank ...
    function.
dr=1;                     % (Used to be r+A) Distance between the lowest ...
    edge of the crank and the reference water surface
%=========================================================================%

f1=@(u)(dr-sqrt(l^2-(r*sin(u))^2))/r;
f2=@(u)cos(u);
Theta_Initial=0;
err=1;
while err>1e-12
    f1n=f1(Theta_Initial);
    f2n=f2(Theta_Initial);
    Theta_Initial=acos(f1n);
    err=abs(f1n-f2n);
end
disp('The Initial Angle is (in radian): ');
disp(Theta_Initial);
disp('In degrees: ');
disp(Theta_Initial/pi*180);
```

B.2.3 Radiation Force Calculation

```
% File name: RadiationKomega
function [bz,az]=RadiationKomega(a,Td)
%=========================================================================%
%==========================Initialization=================================%


%Hydrodynamics initialization
rho=1020;                   % the density of water
g=9.81;                     % acceleration of gravity

%a=5;%0.9533;                   % buoy radius
%A=0.5;                      % The maximum amplitude of water wave, ...
    initialized again in the slider crank function.

Rv=0;                   % Viscous force coefficient
Rf=10;                      % Friction force coefficient



omega=0:0.01:4.4; %when w > 4.4 then ka > 10 in which we don't have ...
    damping data to interpolate for


l2=length(omega);

m=zeros(l2,1);
R=zeros(l2,1);
K=zeros(l2,1);
```

```
Ka=[0 0.05 0.1 0.2 0.3 0.4 0.5 0.6 0.7 0.8 0.9 1.0 1.2 1.4 1.6 1.8 2.0 2.5 ...
    3.0 4.0 5.0 6.0 7.0 8.0 9.0 10.0]';
Amass=[0.8310 0.8764 0.8627 0.7938 0.7157 0.6452 0.5861 0.5381 0.4999 ...
    0.4698 0.4464 0.4284 0.4047 0.3924 0.3871 0.3864 0.3884 0.3988 0.4111 ...
    0.4322 0.4471 0.4574 0.4647 0.4700 0.4740 0.4771]';
Damping=[0 0.1036 0.1816 0.2793 0.3254 0.3410 0.3391 0.3271 0.3098 0.2899 ...
    0.2691 0.2484 0.2096 0.1756 0.1469 0.1229 0.1031 0.0674 0.0452 0.0219 ...
    0.0116 0.0066 0.0040 0.0026 0.0017 0.0012]';
mm=rho*(2*pi/3)*a^3;
minf=0.5;

for j2=1:l2%2*pi*f;              % The angular velocity of water wave

        k=omega(j2)^2/g;                % Wave number for infinite water depth
        Kaq=k*a;                    % ka

        %zw=@(t)A*sin(omega(j2)*t);     % the function of water wave


        %=====================================================================%
        %===Calculating mu, epsilon and kappa through graphical ...
           observation======%


        Mu = interp1(Ka,Amass,Kaq','cubic');
        Ep = interp1(Ka,Damping,Kaq','cubic');
        %kap= interp1(Ka,kappa,Kaq','cubic');

        %=====================================================================%
        %Calculating Coefficients of the Differential Equation of Buoy ...
           Displacement

        m(j2)= mm*(Mu-0.5);
        R(j2)= Rv+Rf+Ep*omega(j2)*mm;
        K(j2)= R(j2)+1i*omega(j2)*m(j2);

end

% mag=abs(K);
% phase=angle(K);
[bs,as] = invfreqs(K,omega,3,4);
% [bz,az] = invfreqz(mag.*exp(j*phase),omega,3,4);
%impulse(tf(b,a)); %Compare with your RIRF
sysc=tf(bs,as)
sysd=c2d(sysc,Td);
[bz1,az1]=tfdata(sysd);
bz=cell2mat(bz1);
az=cell2mat(az1);
end
```

B.2.4 Wave Prediction (Getting the next half period from the already calculated wave excitation force)

```
% File name: Wave_Analysis
% =============Output==============
% Ts are the half periods
% T1s are the time point of zero-crossings
Excitation_Force=Fe(t);
l_Fe=length(Excitation_Force);
i_T=1;
for index=2:l_Fe
    if Excitation_Force(index)*Excitation_Force(index-1)<=0  %0-crossing ...
       detection
        if Excitation_Force(index)>Excitation_Force(index-1)
            pn_flag(i_T)=1;
        else pn_flag(i_T)=0;
        end
        T1_s(i_T)=t(index);
        if i_T>1
            T_s(i_T)=T1_s(i_T)-T1_s(i_T-1);
        else
            T_s(i_T)=0;
        end
        i_T=i_T+1;
    end
end
```

B.2.5 Simulink Model

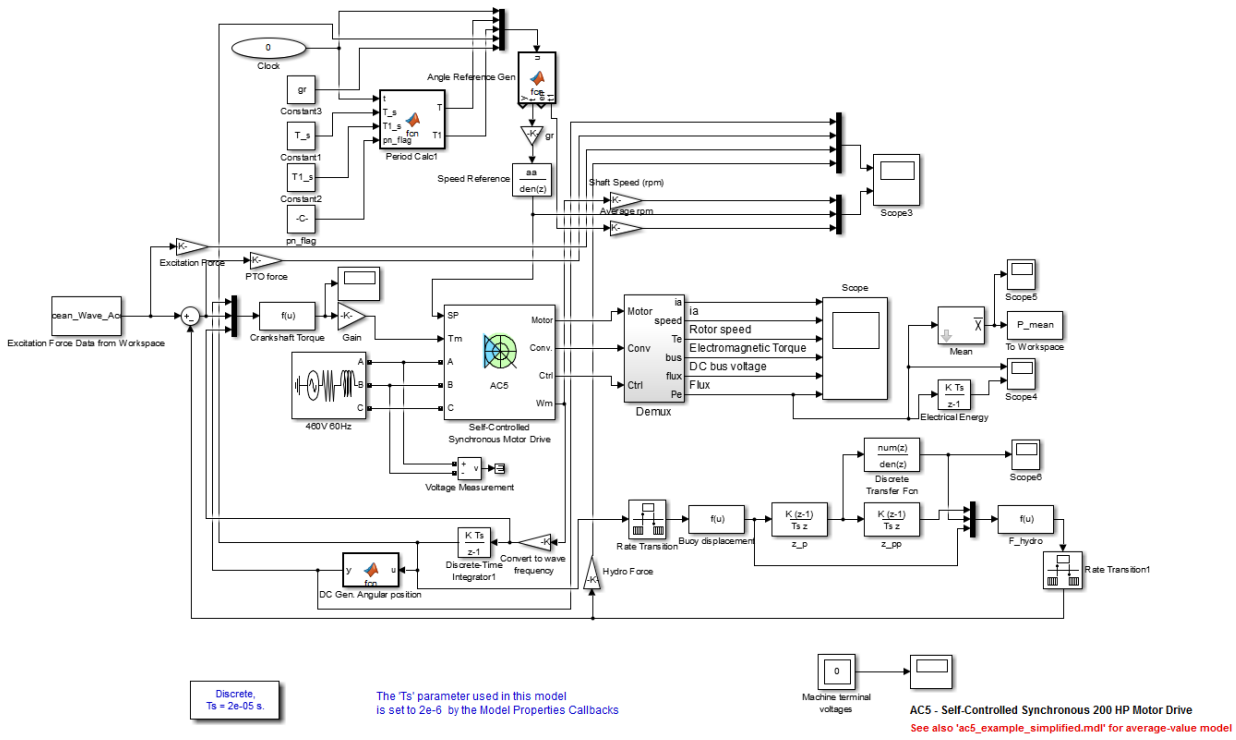

Figure B.2: Simulink model

B.3 Wave Exciation Force Calculation for Irregular Wave with Time-domain Hydrodynamics Analysis and a DC Machine

B.3.1 Main Code

```
clear;clc;close all;
%=========================================================================%
% initial inertia: 10
% initial viscous friction coefficient: 0.32

%=========================================================================%
%Callback for the simulink model
Ts=20e-6; % Sampling time
Td=1e-3; % Discrete Sampling time

%%% setting 1 %%%
gr=110;    % Gear ratio
%======================
aa=20e-6/(.5+20e-6);

%=========================================================================%
%Slider-Crank initialization
r=0.5;                    % Radius of crank. used again in the rk4sys_step ...
    function and slider crank function.
l=1;                      % Length of rod, used again in the slider crank ...
    function.
lambda=r/l;               % used again in the slider crank function.
B=0.01;                  % Viscous friction, used again in the slider ...
    crank function.
J=10;                    % inertia of flywheel, used again in the slider ...
    crank function.
dr=1;                    % (Used to be r+A) Distance between the lowest ...
    edge of the crank and the reference water surface
mcrp=10;                 % Total of mass of piston (or slider) and ...
    connecting rod respectively.

%=========================================================================%
% Hydrodynamics initialization (frequency domain)
delta_omega=0.01;
omega=0.5:delta_omega:1.4;
N=length(omega);
fn=omega/2/pi;% frequencies of the wave components
%%%=======================================%%%
%%% Settings for irregular wave parameters %%%
% Equivalent energy transfer: Hm0=2*sqrt(2)*A  (A is the amplitude of the ...
    regular wave)
Hm0=sqrt(2); % significant wave height of the irregular wave. The same ...
    value is used as that in "Effect of..."
Tp=8; % If this changes, int_S_star has to be recalculated. Peak period of ...
    the irregular wave. In "Effect of...", they used an average period of ...
    6. We can use our own to make the spectrum fit our need.
```

```
%%%=======================================%%%
fp=1/Tp;
g=9.81; % gracity acceleration
rho=1020;% water density

%=========================================================================%
% Choose Spectrum for the System:
flag = 1; % 0 for Breschneider model and 1 for JONSWAP Model

switch flag
    case 0
% ====================  Bretschneider model  ============================%
%         R=(Tp/1.057)^(-4); % These are calculated separately for the ...
   sake of the organing the formula
%         Q=R*Hm0^2/4;% These are calculated separately for the sake of ...
   the organing the formula
%         S=Q*fn.^(-5).*exp(-R*fn.^(-4)); % Bretschneider spectrum ("sea ...
   spectra revisited" or MIT OCW slides)
        S=Hm0^2/4*(1.057*fp)^4*fn.^(-5).*exp(-5/4*(fp./fn).^4); %According ...
           to WEC_Sim_User_Manual_v1.0.pdf
    case 1
% ====================  JONSWAP Model ==================================%
        m0=sqrt(Hm0/4); % wave field variance. See "On control ...".
        %alpha=0.0081; % a given constant which is used in most ...
           references, see "sea spectra revisited".
        gamma=6;% If this changes, int_S_star has to be recalculated. The ...
           average of gamma is 3.3 (see "sea spectra revisited"). ...
           enhancement factor by which the P_M peak energy is multiplied ...
           to get the peak energy value of the spectrum.
        %Increasing gamma has the effect of reducing the spectral bandwidth,
        %thereby increasing periodicity of the wave field. See "On control ...
           ...".
        for i2=1:N
            if fn(i2)<=fp
                sigma=0.07;%if f<fp  sigma is the width factor of the ...
                   enhanced peak, see "sea spectra revisited". The ...
                   numbers are given in "sea spectra revisited".
            elseif fn(i2)>fp
                sigma=0.09;%if f>fp
            end

            %=================================================================%
            % The following eqn uses basic spectrum from "On control ..." ...
               and peak enhancement factor from "Sea_spectra_revisited".
            S(i2)=5*m0/fp*((fp/fn(i2))^5)*exp(-5/4*((fp/fn(i2))^4))  ...
            *gamma^exp(-(fn(i2)-fp)^2/(2*sigma^2*fp^2));
            %=================================================================%
            % The following eqn is according to WEC_Sim_User_Manual_v1.0.pdf
            % integral calculated by Wolframalpha
            switch Tp
                case 6
                    int_S_star=11.9001+20.8213;
                case 7
                    int_S_star=22.0463+38.574;
```

```
                case 8
                    int_S_star=37.61+65.8056;
                case 9
                    int_S_star=60.244+105.408;
                case 10
                    int_S_star=91.8214+160.658;
            end
            alpha=Hm0^2/(int_S_star*16); %int_S_star should be changed ...
               when Tp or gamma changes.
            GAMMA=exp(-((fn(i2)/fp-1)/(sqrt(2)*sigma))^2);
            S(i2)=alpha*g^2/(2*pi)^4*fn(i2)^(-5) ...
            *exp(-5/4*(fp/fn(i2))^4)*gamma^GAMMA;
        end
end
% plot(omega,S)
%=========================================================================%
% Wave elevation and excitation force (time domain)
Start_Time=0;              % time start
End_Time=500;              % final time
Interval=0.01;             % simpling time interval
t=Start_Time:Interval:End_Time;
M=length(t);

%%% setting 2 %%%
a=5; % buoy radius
%======================
c=rho*g*pi*a^2; % a coefficient that is used later
%%% setting 3 %%%
A=sqrt(2*S*delta_omega/2/pi); % calculate amplitude for each wave component
%======================
%%% setting 5 %%%
Phase=pi*rand(1,N); % randomly generate the initial phase of each wave ...
   component
%======================

Ka=[0 0.05 0.1 0.2 0.3 0.4 0.5 0.6 0.7 0.8 0.9 1.0 1.2 1.4 1.6 1.8 2.0 2.5 ...
   3.0 4.0 5.0 6.0 7.0 8.0 9.0 10.0]';
Amass=[0.8310 0.8764 0.8627 0.7938 0.7157 0.6452 0.5861 0.5381 0.4999 ...
   0.4698 0.4464 0.4284 0.4047 0.3924 0.3871 0.3864 0.3884 0.3988 0.4111 ...
   0.4322 0.4471 0.4574 0.4647 0.4700 0.4740 0.4771]';
Damping=[0 0.1036 0.1816 0.2793 0.3254 0.3410 0.3391 0.3271 0.3098 0.2899 ...
   0.2691 0.2484 0.2096 0.1756 0.1469 0.1229 0.1031 0.0674 0.0452 0.0219 ...
   0.0116 0.0066 0.0040 0.0026 0.0017 0.0012]';
len=length(Ka);
kappa=zeros(1,len);
imkap=zeros(1,len);
rekap=zeros(1,len);
mm=rho*(2*pi/3)*a^3;
Sb=rho*g*pi*a^2;%785890;
kappa(1)=1;
imkap(1)= 2*Damping(1)*Ka(1)/3;
rekap(1)= sqrt(kappa(1)^2-imkap(1)^2);
for j=2:len
    kappa(j)= sqrt(4*Damping(j)/(3*pi*Ka(j)));
```

```
    imkap(j)= 2*Damping(j)*Ka(j)/3;
    rekap(j)= sqrt(kappa(j)^2-imkap(j)^2);
end

Kaq=omega.^2/g*a;
kappa_im=zeros(1,N);
kappa_re=zeros(1,N);
kappa_angle=zeros(1,N);
kappa_abs=zeros(1,N);
for i1=1:N
    kappa_abs(i1)=interp1(Ka,kappa,Kaq(i1),'cubic');
    kappa_im(i1)=interp1(Ka,imkap,Kaq(i1),'cubic');
    kappa_re(i1)=interp1(Ka,rekap,Kaq(i1),'cubic');
    kappa_angle(i1)=atan(kappa_im(i1)/kappa_re(i1));
end
%%%
% kap=0.502764572022028;
%%%
% eta=zeros(1,M);
% Fe=zeros(1,M); % initialization for wave force at each time point
Fe=@(t)0;
eta_total=@(t)0;
%%% setting 5 %%%
% omega=2*pi/6*ones(1,N);
% kappa_angle=0;
%======================
for i=1:N
    eta{i}=@(t)A(i)*sin(omega(i)*t+Phase(i)+kappa_angle(i));
    Fe_components{i}=@(t)c*kappa_abs(i)*eta{i}(t);
    Fe=@(t)Fe(t)+Fe_components{i}(t);
    eta_total=@(t)eta_total(t)+eta{i}(t);
end

figure;
% subplot(2,1,1)
% plot(t,eta);
% grid
% title('wave elevation')

% subplot(2,1,2)
plot(t,Fe(t));
grid
title('excitation force')
% hold on;
figure;
plot(t,eta_total(t));
grid
title('wave elevation')
Ocean_Wave_AccP.signals.values=Fe(t)';
Ocean_Wave_AccP.time=t';


%Call to find initial angle
Theta_Initial=Initial_Angle_Solver();
```

```
[bz,az]=RadiationKomega(a,Td);
Wave_Analysis;
```

B.3.2 Initial Angle Solver

```
% File name: Initial_Angle_Solver
function Theta_Initial=Initial_Angle_Solver()
format long;
%=========================================================================%
%Slider-Crank initialization
r=0.5;                      % Radius of crank. used again in the rk4sys_step ...
   function and slider crank function.
l=1;                        % Length of rod, used again in the slider crank ...
   function.
dr=1;                     % (Used to be r+A) Distance between the lowest ...
   edge of the crank and the reference water surface
%=========================================================================%

f1=@(u)(dr-sqrt(l^2-(r*sin(u))^2))/r;
f2=@(u)cos(u);
Theta_Initial=0;
err=1;
while err>1e-12
    f1n=f1(Theta_Initial);
    f2n=f2(Theta_Initial);
    Theta_Initial=acos(f1n);
    err=abs(f1n-f2n);
end
disp('The Initial Angle is (in radian): ');
disp(Theta_Initial);
disp('In degrees: ');
disp(Theta_Initial/pi*180);
```

B.3.3 Radiation Force Calculation

```
% File name: RadiationKomega
function [bz,az]=RadiationKomega(a,Td)
%=========================================================================%
%==========================Initialization=================================%


%Hydrodynamics initialization
rho=1020;                   % the density of water
g=9.81;                     % acceleration of gravity

%a=5;%0.9533;                   % buoy radius
%A=0.5;                      % The maximum amplitude of water wave, ...
   initialized again in the slider crank function.

Rv=0;                   % Viscous force coefficient
```

```
Rf=10;                      % Friction force coefficient


omega=0:0.01:4.4; %when w > 4.4 then ka > 10 in which we don't have ...
    damping data to interpolate for


l2=length(omega);

m=zeros(l2,1);
R=zeros(l2,1);
K=zeros(l2,1);

Ka=[0 0.05 0.1 0.2 0.3 0.4 0.5 0.6 0.7 0.8 0.9 1.0 1.2 1.4 1.6 1.8 2.0 2.5 ...
    3.0 4.0 5.0 6.0 7.0 8.0 9.0 10.0]';
Amass=[0.8310 0.8764 0.8627 0.7938 0.7157 0.6452 0.5861 0.5381 0.4999 ...
    0.4698 0.4464 0.4284 0.4047 0.3924 0.3871 0.3864 0.3884 0.3988 0.4111 ...
    0.4322 0.4471 0.4574 0.4647 0.4700 0.4740 0.4771]';
Damping=[0 0.1036 0.1816 0.2793 0.3254 0.3410 0.3391 0.3271 0.3098 0.2899 ...
    0.2691 0.2484 0.2096 0.1756 0.1469 0.1229 0.1031 0.0674 0.0452 0.0219 ...
    0.0116 0.0066 0.0040 0.0026 0.0017 0.0012]';
mm=rho*(2*pi/3)*a^3;
minf=0.5;

for j2=1:l2%2*pi*f;             % The angular velocity of water wave

        k=omega(j2)^2/g;              % Wave number for infinite water depth
        Kaq=k*a;                    % ka

        %zw=@(t)A*sin(omega(j2)*t);    % the function of water wave


        %=========================================================================%
        %===Calculating mu, epsilon and kappa through graphical ...
            observation======%


        Mu = interp1(Ka,Amass,Kaq','cubic');
        Ep = interp1(Ka,Damping,Kaq','cubic');
        %kap= interp1(Ka,kappa,Kaq','cubic');

        %=========================================================================%
        %Calculating Coefficients of the Differential Equation of Buoy ...
            Displacement

        m(j2)= mm*(Mu-0.5);
        R(j2)= Rv+Rf+Ep*omega(j2)*mm;
        K(j2)= R(j2)+1i*omega(j2)*m(j2);

end

% mag=abs(K);
% phase=angle(K);
```

```
[bs,as] = invfreqs(K,omega,3,4);
% [bz,az] = invfreqz(mag.*exp(j*phase),omega,3,4);
%impulse(tf(b,a)); %Compare with your RIRF
sysc=tf(bs,as)
sysd=c2d(sysc,Td);
[bz1,az1]=tfdata(sysd);
bz=cell2mat(bz1);
az=cell2mat(az1);
end
```

B.3.4 Wave Prediction (Getting the next half period from the already calculated wave excitation force)

```
% File name: Wave_Analysis
% =============Output==============
% Ts are the half periods
% T1s are the time point of zero-crossings
Excitation_Force=Fe(t);
l_Fe=length(Excitation_Force);
i_T=1;
for index=2:l_Fe
    if Excitation_Force(index)*Excitation_Force(index-1)<=0  %0-crossing ...
       detection
        if Excitation_Force(index)>Excitation_Force(index-1)
            pn_flag(i_T)=1;
        else pn_flag(i_T)=0;
        end
        T1_s(i_T)=t(index);
        if i_T>1
            T_s(i_T)=T1_s(i_T)-T1_s(i_T-1);
        else
            T_s(i_T)=0;
        end
        i_T=i_T+1;
    end
end
```

B.3.5 Simulink Model

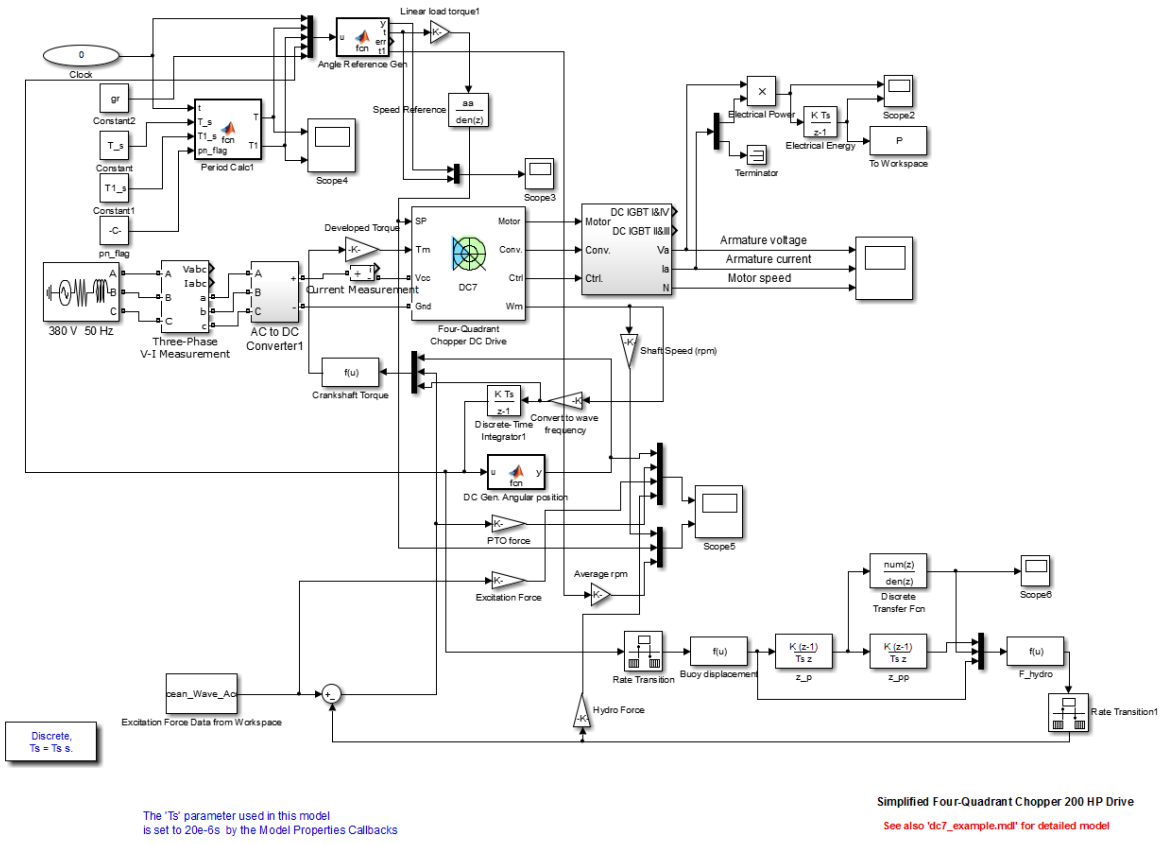

Figure B.3: Simulink model

B.4 Wave Exciation Force Calculation for Irregular Wave with Time-domain Hydrodynamics Analysis and an AC Machine

B.4.1 Main Code

```
clear;clc;close all;
%=========================================================================%
% initial inertia: 10
% initial viscous friction coefficient: 0.32

%=========================================================================%
%Callback for the simulink model
Ts=20e-6; % Sampling time
Td=1e-3; % Discrete Sampling time

%%% setting 1 %%%
gr=110;    % Gear ratio
%======================
aa=20e-6/(.5+20e-6);
```

```
%=========================================================================%
%Slider-Crank initialization
r=0.5;                      % Radius of crank. used again in the rk4sys_step ...
   function and slider crank function.
l=1;                        % Length of rod, used again in the slider crank ...
   function.
lambda=r/l;                 % used again in the slider crank function.
B=0.01;                    % Viscous friction, used again in the slider ...
   crank function.
J=10;                      % inertia of flywheel, used again in the slider ...
   crank function.
dr=1;                      % (Used to be r+A) Distance between the lowest ...
   edge of the crank and the reference water surface
mcrp=10;                   % Total of mass of piston (or slider) and ...
   connecting rod respectively.

%=========================================================================%
% Hydrodynamics initialization (frequency domain)
delta_omega=0.01;
omega=0.5:delta_omega:1.4;
N=length(omega);
fn=omega/2/pi;% frequencies of the wave components
%%%=======================================%%%
%%% Settings for irregular wave parameters %%%
% Equivalent energy transfer: Hm0=2*sqrt(2)*A  (A is the amplitude of the ...
   regular wave)
Hm0=sqrt(2); % significant wave height of the irregular wave. The same ...
   value is used as that in "Effect of..."
Tp=8; % If this changes, int_S_star has to be recalculated. Peak period of ...
   the irregular wave. In "Effect of...", they used an average period of ...
   6. We can use our own to make the spectrum fit our need.
%%%=======================================%%%
fp=1/Tp;
g=9.81; % gracity acceleration
rho=1020;% water density

%=========================================================================%
% Choose Spectrum for the System:
flag = 1; % 0 for Breschneider model and 1 for JONSWAP Model

switch flag
    case 0
% ====================  Bretschneider model  ============================%
%         R=(Tp/1.057)^(-4); % These are calculated separately for the ...
   sake of the organing the formula
%         Q=R*Hm0^2/4;% These are calculated separately for the sake of ...
   the organing the formula
%         S=Q*fn.^(-5).*exp(-R*fn.^(-4)); % Bretschneider spectrum ("sea ...
   spectra revisited" or MIT OCW slides)
        S=Hm0^2/4*(1.057*fp)^4*fn.^(-5).*exp(-5/4*(fp./fn).^4); %According ...
           to WEC_Sim_User_Manual_v1.0.pdf
    case 1
% ====================  JONSWAP Model ==================================%
        m0=sqrt(Hm0/4); % wave field variance. See "On control ...".
```

```
        %alpha=0.0081; % a given constant which is used in most ...
           references, see "sea spectra revisited".
        gamma=6;% If this changes, int_S_star has to be recalculated. The ...
           average of gamma is 3.3 (see "sea spectra revisited"). ...
           enhancement factor by which the P_M peak energy is multiplied ...
           to get the peak energy value of the spectrum.
        %Increasing gamma has the effect of reducing the spectral bandwidth,
        %thereby increasing periodicity of the wave field. See "On control ...
           ...".
        for i2=1:N
            if fn(i2)<=fp
                sigma=0.07;%if f<fp  sigma is the width factor of the ...
                   enhanced peak, see "sea spectra revisited". The ...
                   numbers are given in "sea spectra revisited".
            elseif fn(i2)>fp
                sigma=0.09;%if f>fp
            end
            %=====================================================================%
            % The following eqn uses basic spectrum from "On control ..." ...
               and peak enhancement factor from "Sea_spectra_revisited".
            S(i2)=5*m0/fp*((fp/fn(i2))^5)*exp(-5/4*((fp/fn(i2))^4)) ...
        *gamma^exp(-(fn(i2)-fp)^2/(2*sigma^2*fp^2));
            %=====================================================================%
            % The following eqn is according to WEC_Sim_User_Manual_v1.0.pdf
            % integral calculated by Wolframalpha

            switch Tp
                case 6
                    int_S_star=11.9001+20.8213;
                case 7
                    int_S_star=22.0463+38.574;
                case 8
                    int_S_star=37.61+65.8056;
                case 9
                    int_S_star=60.244+105.408;
                case 10
                    int_S_star=91.8214+160.658;
            end
            alpha=Hm0^2/(int_S_star*16); %int_S_star should be changed ...
               when Tp or gamma changes.
            GAMMA=exp(-((fn(i2)/fp-1)/(sqrt(2)*sigma))^2);
            S(i2)=alpha*g^2/(2*pi)^4*fn(i2)^(-5) ...
        *exp(-5/4*(fp/fn(i2))^4)*gamma^GAMMA;
        end
end
% plot(omega,S)
%=========================================================================%
% Wave elevation and excitation force (time domain)
Start_Time=0;              % time start
End_Time=700;              % final time
Interval=0.01;             % simpling time interval
t=Start_Time:Interval:End_Time;
M=length(t);
```

```
%%% setting 2 %%%
a=5; % buoy radius
%======================
c=rho*g*pi*a^2; % a coefficient that is used later
%%% setting 3 %%%
A=sqrt(2*S*delta_omega/2/pi); % calculate amplitude for each wave component
%======================
%%% setting 5 %%%
Phase=2*pi*rand(1,N); % randomly generate the initial phase of each wave ...
    component
%======================

Ka=[0 0.05 0.1 0.2 0.3 0.4 0.5 0.6 0.7 0.8 0.9 1.0 1.2 1.4 1.6 1.8 2.0 2.5 ...
    3.0 4.0 5.0 6.0 7.0 8.0 9.0 10.0]';
Amass=[0.8310 0.8764 0.8627 0.7938 0.7157 0.6452 0.5861 0.5381 0.4999 ...
    0.4698 0.4464 0.4284 0.4047 0.3924 0.3871 0.3864 0.3884 0.3988 0.4111 ...
    0.4322 0.4471 0.4574 0.4647 0.4700 0.4740 0.4771]';
Damping=[0 0.1036 0.1816 0.2793 0.3254 0.3410 0.3391 0.3271 0.3098 0.2899 ...
    0.2691 0.2484 0.2096 0.1756 0.1469 0.1229 0.1031 0.0674 0.0452 0.0219 ...
    0.0116 0.0066 0.0040 0.0026 0.0017 0.0012]';
len=length(Ka);
kappa=zeros(1,len);
imkap=zeros(1,len);
rekap=zeros(1,len);
mm=rho*(2*pi/3)*a^3;
Sb=rho*g*pi*a^2;%785890;
kappa(1)=1;
imkap(1)= 2*Damping(1)*Ka(1)/3;
rekap(1)= sqrt(kappa(1)^2-imkap(1)^2);
for j=2:len
    kappa(j)= sqrt(4*Damping(j)/(3*pi*Ka(j)));
    imkap(j)= 2*Damping(j)*Ka(j)/3;
    rekap(j)= sqrt(kappa(j)^2-imkap(j)^2);
end

Kaq=omega.^2/g*a;
kappa_im=zeros(1,N);
kappa_re=zeros(1,N);
kappa_angle=zeros(1,N);
kappa_abs=zeros(1,N);
for i1=1:N
    kappa_abs(i1)=interp1(Ka,kappa,Kaq(i1),'cubic');
    kappa_im(i1)=interp1(Ka,imkap,Kaq(i1),'cubic');
    kappa_re(i1)=interp1(Ka,rekap,Kaq(i1),'cubic');
    kappa_angle(i1)=atan(kappa_im(i1)/kappa_re(i1));
end
%%%
% kap=0.502764572022028;
%%%
% eta=zeros(1,M);
% Fe=zeros(1,M); % initialization for wave force at each time point
Fe=@(t)0;
eta_total=@(t)0;
%%% setting 5 %%%
```

```
% omega=2*pi/6*ones(1,N);
% kappa_angle=0;
%======================
for i=1:N
    eta{i}=@(t)A(i)*sin(omega(i)*t+Phase(i)+kappa_angle(i));
    Fe_components{i}=@(t)c*kappa_abs(i)*eta{i}(t);
    Fe=@(t)Fe(t)+Fe_components{i}(t);
    eta_total=@(t)eta_total(t)+eta{i}(t);
end

figure;
% subplot(2,1,1)
% plot(t,eta);
% grid
% title('wave elevation')

% subplot(2,1,2)
plot(t,Fe(t));
grid
title('excitation force')
% hold on;
figure;
plot(t,eta_total(t));
grid
title('wave elevation')
Ocean_Wave_AccP.signals.values=Fe(t)';
Ocean_Wave_AccP.time=t';

%Call to find initial angle
Theta_Initial=Initial_Angle_Solver();
[bz,az]=RadiationKomega(a,Td);
Wave_Analysis;
```

B.4.2 Initial Angle Solver

```
% File name: Initial_Angle_Solver
function Theta_Initial=Initial_Angle_Solver()
format long;
%=========================================================================%
%Slider-Crank initialization
r=0.5;                      % Radius of crank. used again in the rk4sys_step ...
   function and slider crank function.
l=1;                        % Length of rod, used again in the slider crank ...
   function.
dr=1;                     % (Used to be r+A) Distance between the lowest ...
   edge of the crank and the reference water surface
%=========================================================================%

f1=@(u)(dr-sqrt(l^2-(r*sin(u))^2))/r;
f2=@(u)cos(u);
Theta_Initial=0;
err=1;
```

```
while err>1e-12
    f1n=f1(Theta_Initial);
    f2n=f2(Theta_Initial);
    Theta_Initial=acos(f1n);
    err=abs(f1n-f2n);
end
disp('The Initial Angle is (in radian): ');
disp(Theta_Initial);
disp('In degrees: ');
disp(Theta_Initial/pi*180);
```

B.4.3 Radiation Force Calculation

```
% File name: RadiationKomega
function [bz,az]=RadiationKomega(a,Td)
%=========================================================================%
%============================Initialization===============================%


%Hydrodynamics initialization
rho=1020;                   % the density of water
g=9.81;                     % acceleration of gravity

%a=5;%0.9533;                   % buoy radius
%A=0.5;                      % The maximum amplitude of water wave, ...
   initialized again in the slider crank function.

Rv=0;                   % Viscous force coefficient
Rf=10;                      % Friction force coefficient



omega=0:0.01:4.4; %when w > 4.4 then ka > 10 in which we don't have ...
   damping data to interpolate for


l2=length(omega);

m=zeros(l2,1);
R=zeros(l2,1);
K=zeros(l2,1);

Ka=[0 0.05 0.1 0.2 0.3 0.4 0.5 0.6 0.7 0.8 0.9 1.0 1.2 1.4 1.6 1.8 2.0 2.5 ...
   3.0 4.0 5.0 6.0 7.0 8.0 9.0 10.0]';
Amass=[0.8310 0.8764 0.8627 0.7938 0.7157 0.6452 0.5861 0.5381 0.4999 ...
   0.4698 0.4464 0.4284 0.4047 0.3924 0.3871 0.3864 0.3884 0.3988 0.4111 ...
   0.4322 0.4471 0.4574 0.4647 0.4700 0.4740 0.4771]';
Damping=[0 0.1036 0.1816 0.2793 0.3254 0.3410 0.3391 0.3271 0.3098 0.2899 ...
   0.2691 0.2484 0.2096 0.1756 0.1469 0.1229 0.1031 0.0674 0.0452 0.0219 ...
   0.0116 0.0066 0.0040 0.0026 0.0017 0.0012]';
mm=rho*(2*pi/3)*a^3;
minf=0.5;
```

```
for j2=1:l2%2*pi*f;              % The angular velocity of water wave

        k=omega(j2)^2/g;               % Wave number for infinite water depth
        Kaq=k*a;                    % ka

        %zw=@(t)A*sin(omega(j2)*t);    % the function of water wave


        %=====================================================================%
        %===Calculating mu, epsilon and kappa through graphical ...
           observation======%


        Mu = interp1(Ka,Amass,Kaq','cubic');
        Ep = interp1(Ka,Damping,Kaq','cubic');
        %kap= interp1(Ka,kappa,Kaq','cubic');

        %=====================================================================%
        %Calculating Coefficients of the Differential Equation of Buoy ...
           Displacement

        m(j2)= mm*(Mu-0.5);
        R(j2)= Rv+Rf+Ep*omega(j2)*mm;
        K(j2)= R(j2)+1i*omega(j2)*m(j2);

end

% mag=abs(K);
% phase=angle(K);
[bs,as] = invfreqs(K,omega,3,4);
% [bz,az] = invfreqz(mag.*exp(j*phase),omega,3,4);
%impulse(tf(b,a)); %Compare with your RIRF
sysc=tf(bs,as)
sysd=c2d(sysc,Td);
[bz1,az1]=tfdata(sysd);
bz=cell2mat(bz1);
az=cell2mat(az1);
end
```

B.4.4 Wave Prediction (Getting the next half period from the already calculated wave excitation force)

```
% File name: Wave_Analysis
% =============Output==============
% Ts are the half periods
% T1s are the time point of zero-crossings
Excitation_Force=Fe(t);
l_Fe=length(Excitation_Force);
i_T=1;
for index=2:l_Fe
    if Excitation_Force(index)*Excitation_Force(index-1)<=0  %0-crossing ...
```

```
        detection
         if Excitation_Force(index)>Excitation_Force(index-1)
             pn_flag(i_T)=1;
         else pn_flag(i_T)=0;
         end
         T1_s(i_T)=t(index);
         if i_T>1
             T_s(i_T)=T1_s(i_T)-T1_s(i_T-1);
         else
             T_s(i_T)=0;
         end
         i_T=i_T+1;
    end
end
```

B.4.5 Simulink Model

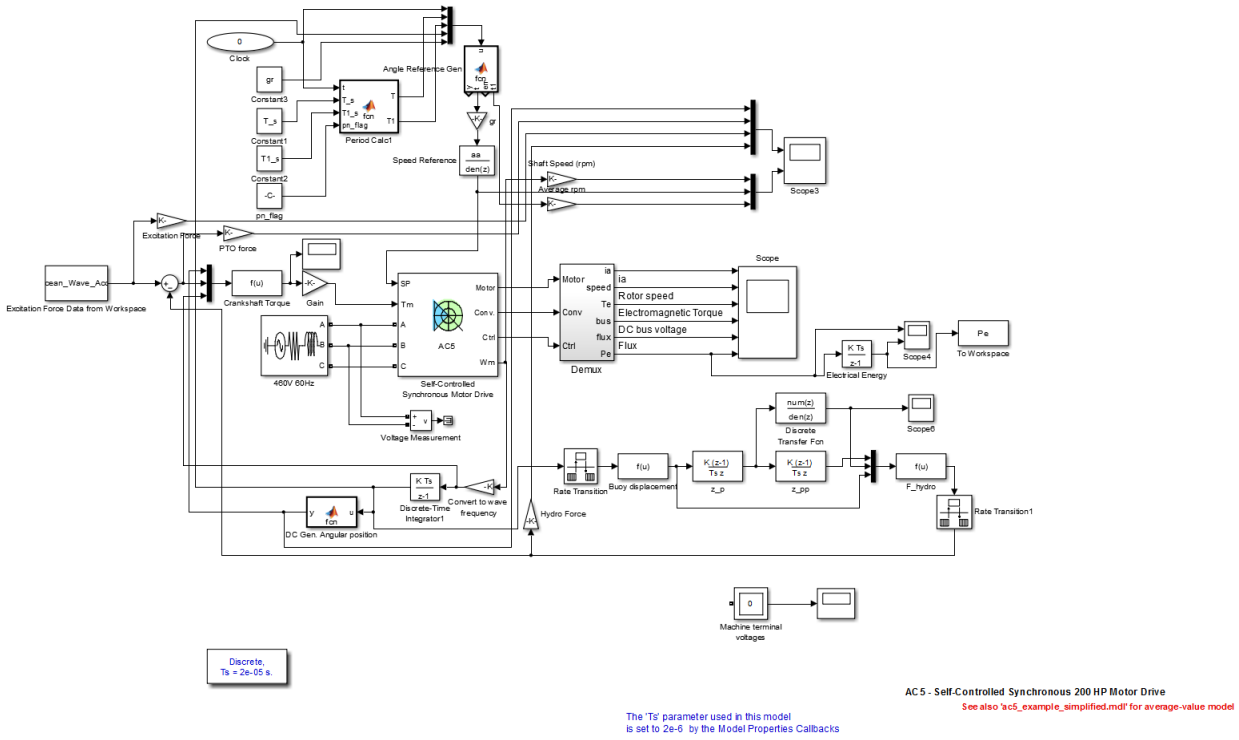

Figure B.4: Simulink model